Chapter 8
Microstructural Evolution of the Interdiffusion Zone

In this chapter, previously unknown behavior of marker plane is shown. In most of the cases, we find the markers along one particular plane; however, in certain condition, these might spread. Sometimes, markers split into more than one planes. A characteristic microstructural feature is found to develop depending on the number and location of the marker planes. This led to development of a physico-chemical approach explaining the microstructural evolution in the interdiffusion zone.

As already discussed in Chap. 6, the discovery of the Kirkendall effect [1, 2] is one of the most important developments in the area of solid-state diffusion. This helped to validate the vacancy-mediated substitutional diffusion. For long, it was known that the markers accumulate at a single plane with a fixed composition. However, sometimes, an unusual behavior of the marker plane has been reported in the literature on this subject. Bastin and Rieck [3] placed W wire at the interface of a Ni/Ti diffusion couple before annealing it at 800 °C for 72 h. Three phases, Ti_2Ni, TiNi, and $TiNi_3$, were grown in the interdiffusion zone. Surprisingly, the authors found pieces of broken W wire in different phases, as if these markers tried to move to different planes simultaneously. Much later, in 1993, Shimozaki et al. [4] reported another unusual behavior in the β′-AuZn phase grown by interdiffusion in the $Au/Au_{0.36}Zn_{0.64}$ diffusion couple. As discussed in Chap. 6, the position of the marker plane could be detected by the presence of a line of pores that developed because of the negative surface (such as scratches or by the presence of debris left on the metallographically prepared bonding surfaces). In general, the markers used to detect the Kirkendall plane are also found along with these on the same plane. Shimozaki et al. used 5-μm-diameter W wire as an inert marker. To their surprise, they found the wires at one plane and the traces (pores caused by scratches or debris) of the original interface at another plane. In both cases, the actual reason for such behavior was not known. In the meantime, following theoretical analysis, Cornet and Calais [5] and van Loo et al. [6] described the possibility of finding more than one Kirkendall marker plane in an interdiffusion zone. In their analysis, they considered a diffusion couple of α and β with a single interface between them. First, they showed that depending on the initial composition of the end members, the same interface can act as both a source and a sink for vacancies when one particular

A. Paul et al., *Thermodynamics, Diffusion and the Kirkendall Effect in Solids*,
DOI: 10.1007/978-3-319-07461-0_8,

component diffuses at a faster rate in both the phases. If $D_A/D_B > 1$ in one phase and $D_A/D_B < 1$ in the other phase, depending on the initial end-member compositions, there could be two Kirkendall planes present in the interdiffusion zone. In that case, the inert markers placed at the initial contact plane have to split and will accumulate at two different planes: one in the α phase and the other in the β phase. In fact, we should consider a marker plane in each phase. Depending on the end-member compositions, the intrinsic diffusion coefficients and the interdiffusion coefficients, it is possible to actually find one or more than one marker planes. After the manuscript published by Shimozaki et al. extensive studies were conducted in several systems including the Ni–Ti and the Au–Zn systems in order to demonstrate the previously unknown behavior of the marker planes [7–13]. Now, we know that the inert markers could be stable to be found in one plane. Under certain circumstances, we might notice some unstable behavior, in which, instead of accumulation in one plane, the markers might spread over a wider area. Depending on the end-member compositions and diffusivities, more than one plane also could be found in a single phase or in different phases. Based on which, a physico-chemical approach is developed to explain the morphologies in a multiphase interdiffusion zone depending on the presence of a single or multiple Kirkendall planes.

8.1 Stable, Unstable, and Multiple Kirkendall Marker Planes

In Chap. 6, we have seen that the intrinsic diffusion coefficients can be estimated over the composition range using an incremental diffusion couple by making several diffusion couples with different end members or from a single diffusion couple by making a multifoil diffusion couple. Once the intrinsic diffusion coefficients (D_A and D_B) are calculated, the velocity at a different composition in a particular diffusion couple can be determined from the knowledge of these diffusion parameters at different compositions and the concentration gradient measured at those compositions following the relation as expressed in Eq. 6.61

$$v_K = \bar{v}_B (D_B - D_A) \left(\frac{\partial C_B}{\partial x} \right)_K \tag{8.1}$$

The velocity of the Kirkendall plane (or the composition of the Kirkendall marker plane) can also be determined directly by locating the initial contact plane x_o and the Kirkendall marker plane x_K from the relation as expressed in Eq. 6.64

$$v_K = \frac{x_K - x_o}{2t} = \frac{x_K}{2t} \tag{8.2}$$

Therefore, at the intersection point of these two lies the location of the Kirkendall marker plane, since both have the same velocity at this plane [7, 8]. To explain

further in a simplified system, let us consider, the constant molar volume of a system, such that $v_A = v_B = v_m$ and a constant interdiffusion coefficient $\tilde{D}$ over the whole concentration range. Therefore, Fick's second law reduces to

$$\frac{\partial N_B}{\partial t} = \tilde{D}\frac{\partial^2 N_B}{\partial x^2} \tag{8.3}$$

The solution of Eq. 8.3 with respect to error function can be written as [7, 8, 10]

$$N_B = \frac{1}{2}\mathrm{erfc}\left(\frac{x}{2\sqrt{\tilde{D}t}}\right) \tag{8.4}$$

For a constant molar volume, Eq. 8.1 can be written as

$$v = (D_B - D_A)\frac{\partial N_B}{\partial x} \tag{8.5}$$

Further, the Darken relation (Eq. 6.65) can be expressed as

$$\tilde{D} = N_A D_B + N_B D_A \tag{8.6}$$

If we would like to consider a constant ratio of diffusivities, Eq. 8.5, with the help of Eq. 8.6 can be written as

$$v = \tilde{D}\left(\frac{\frac{D_B}{D_A} - 1}{N_A\frac{D_B}{D_A} + N_B}\right)\frac{\partial N_B}{\partial x} \tag{8.7}$$

With the help of Eq. 8.4, Eq. 8.7 can be written as

$$v = \tilde{D}\left(\frac{\frac{D_B}{D_A} - 1}{N_A\frac{D_B}{D_A} + N_B}\right)\left(\frac{-1}{\sqrt{\pi}}\frac{1}{2\sqrt{\tilde{D}t}}\right)\exp\left[-\left(\frac{x}{2\sqrt{\tilde{D}t}}\right)^2\right] \tag{8.8}$$

After plotting v versus x using Eq. 8.8, the location of the Kirkendall plane can be rationalized by the intersection of the straight line—expressed by Eq. 8.2—that goes through $x = 0$. The velocity diagram, as shown in Fig. 8.1, is estimated for $\tilde{D} = 10^{-14}\,\mathrm{m^2/s}$, $D_A/D_B = 3$, $t = 10^6$ s and for the constant molar volume [7, 10].

Note that in an actual case, the ratios of the diffusivities are not constant over the whole composition range and even the molar volume might change drastically. In that case, Eqs. 8.1 and 8.2 should be used to construct the velocity curve. Cornet and Calais [5] explained the possibility of finding multiple Kirkendall marker planes in a theoretical analysis. Much later, the group of van Loo [7–13] conducted extensive experimental studies to show the different possibilities of the marker planes and explained these behaviors with the help of theoretical analysis that has been developed based on the work by Cornet and Calais [5]. Now, we know that a

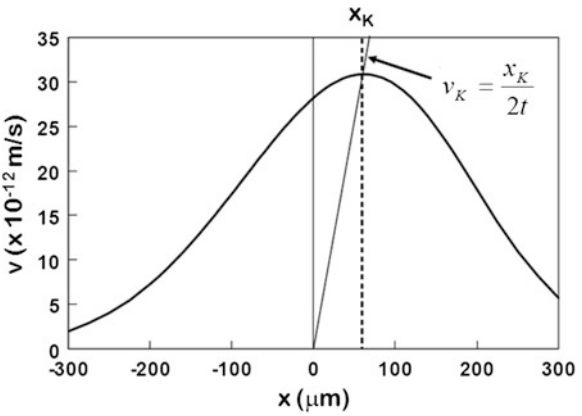

Fig. 8.1 Velocity diagram showing the location of the Kirkendall marker plane [7]

stable marker plane can be present in a system such that all the inert markers accumulate along a single composition indicating the position of the Kirkendall marker plane. On the other hand, markers can be unstable such that they spread over a composition or region in the interdiffusion zone. In a few special cases, markers have been known to bifurcate or trifurcate. There is a possibility of bifurcation in a single phase or in two different phases.

Before showing the experimental results, it is necessary to understand the condition in which different kinds of behavior could be found [7, 8]. We consider a system where in the A-rich side A has a higher diffusion rate compared to B and in the B-rich side B has a higher diffusion rate compared to A. In such a case, according to Eq. 8.1, as shown in Fig. 8.2, the velocity will have a negative value in the A-rich side and positive values in the B-rich side. We have considered the left-hand side of the diffusion couple as being A-rich and the right-hand side of the couple as being B-rich. Following, the number and nature of the marker plane will depend on the location of the intersection on the velocity curve by the straight line determined by Eq. 8.2. Depending on the end-member compositions, the interdiffusion coefficients and the intrinsic diffusion coefficients, the straight line estimated from the position of the marker plane might intersect the velocity curve at a point, where it has a negative gradient $dv/dx < 0$. This point is shown in Fig. 8.2a. In this case, it will have a stable marker plane such that all the markers will accumulate at this Kirkendall marker plane located at x_K. At the very initial stage, if for any reason, the markers move ahead of this plane, they will slow down due to lower velocity and come back to the stable plane. On the other hand, if the markers are left behind this plane, they will move faster because of the higher velocity and drift to the marker plane. Therefore, the marker plane acts as the attractor for the markers to accumulate the inert particles from the nearby positions.

As shown in Fig. 8.2b, by changing the end-member compositions in the same system, the position of the initial contact plane $x_o = 0$ might move such that the straight line intersects the velocity curve at a point where it has a positive gradient

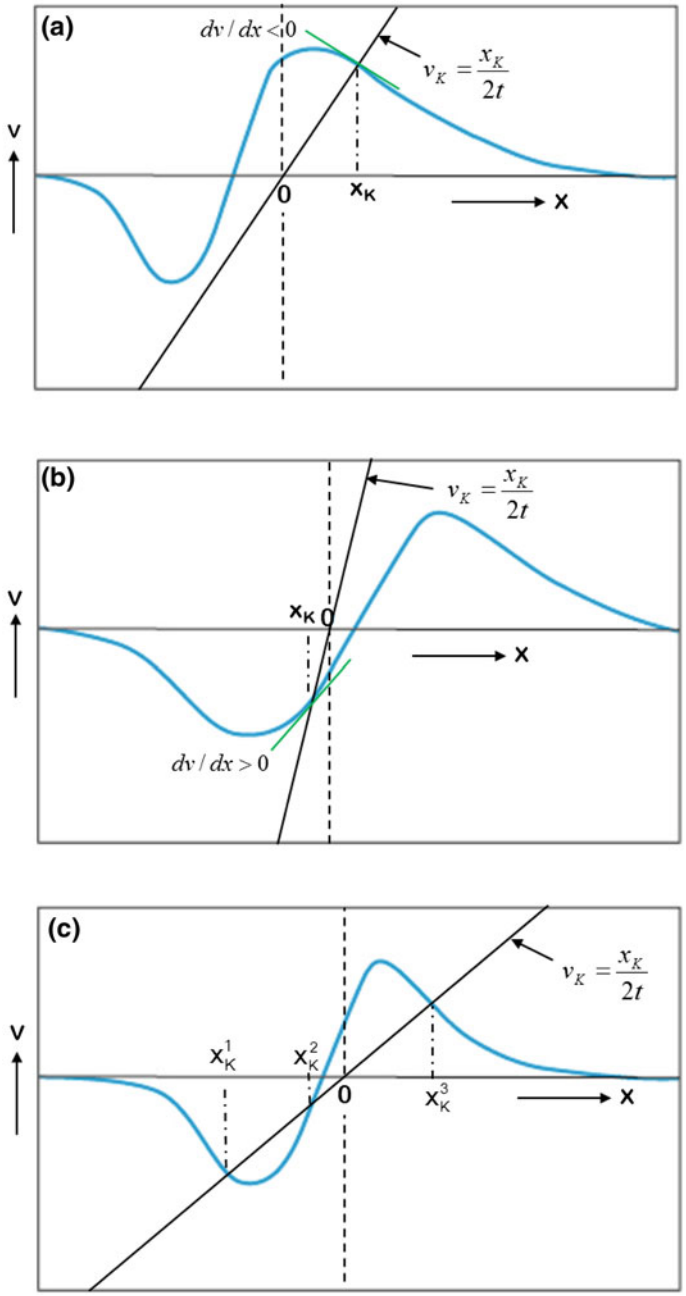

Fig. 8.2 Imaginary velocity diagrams showing the possibility of finding **a** a stable marker plane, **b** an unstable marker plane, and **c** bifurcation of the marker plane in the same system [7]

$dv/dx > 0$. It should be noted here that the slope of the line, $v_K = \frac{x_K}{2t}$ also changes with the change in end-member compositions. Following a similar line of discussion, the stability of the movement of the inert markers can be explained. At the very initial stage, for any perturbation, if the markers are left behind, they will slow down because of lower velocity. On the other hand, if the markers move ahead, they will move faster to go even further away. Therefore, it will show unstable marker behavior, where the markers will be spread over a larger area.

In another diffusion couple with different end members, a situation might arise where the straight line intersects the velocity curve at three points, as shown in Fig. 8.2c. An unstable marker plane is present at x_K^2 between two stable planes at x_K^1 and x_K^3. At the very initial stage, since the markers move away from the unstable marker plane, the markers will be attracted by the stable planes. Therefore, in this diffusion couple, two stable marker planes—that is the bifurcation of the marker plane—will be found.

The conditions of finding stable and unstable Kirkendall marker planes were examined experimentally in the Ni–Pd and Fe–Pd systems, as shown in Fig. 8.3 [9]. ThO_2 particles were used as inert markers. As discussed in the previous chapter, the velocity curves were determined following a multifoil technique. The intersection points—indicating the location of the Kirkendall marker planes—are found by plotting the straight line from the estimated location of the initial contact plane and the known location of the Kirkendall marker plane. It can be seen that $dv/dx < 0$ at the point of intersection in the Ni–Pd system, where a stable marker plane is found. On the other hand, in the Fe–Pd system $dv/dx > 0$ at the point of intersection and it has an unstable Kirkendall plane. In the Fe–Pd system, since there is no particular marker plane present, a plane approximately in the middle of the marker region was considered for the construction of the velocity diagram.

Experimental evidence indicating the presence of stable, unstable, and the bifurcation of the marker plane was found in the β′-AuZn phase in the diffusion couples with different end-member compositions [8]. From the tracer diffusion data available in the literature published on the subject, it was known that Au is the faster diffusing component in the Au-rich and Zn is the faster diffusing component in the Zn-rich side of this phase. Therefore, it was expected to find the situations, as explained in Fig. 8.2. As shown in Fig. 8.4, in a diffusion couple of $Au_{0.66}Zn_{0.34}/Au_{0.34}Zn_{0.66}$, a stable Kirkendall marker plane was found. As presented in Fig. 8.5, by changing the end-member compositions, an unstable Kirkendall marker plane was found in the same phase in a $Au_{0.70}Zn_{0.30}/Au_{0.40}Zn_{0.60}$ diffusion couple. The Kirkendall marker location—as shown in a rectangle denoted by B in Fig. 8.5b—is shown in Fig. 8.5c where an array of markers are to be seen spreading over a region. By changing the end-member compositions of the diffusion couple, as shown in Fig. 8.6, the bifurcation of the Kirkendall marker plane was found. One Kirkendall plane was found in the Au-rich and another in the Zn-rich side of the β′-AuZn phase.

However, rationalization with the help of a velocity diagram was not possible because of difficulties in determining the intrinsic diffusion coefficients over the

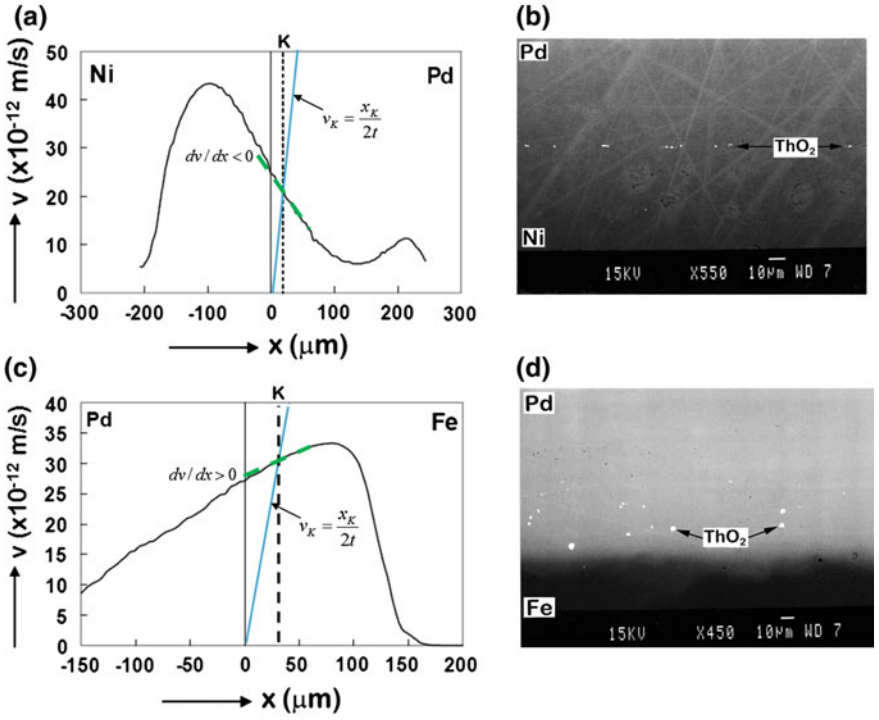

Fig. 8.3 **a** Velocity diagram constructed experimentally in the Ni–Pd system and **b** experimentally found a stable marker plane. **c** Velocity diagram constructed experimentally in the Fe–Pd system and **d** experimentally found unstable marker plane [9]

whole composition range in the β′-AuZn phase. Absence of the data on lattice parameter variation and Zn evaporation during melting complicated the analysis. Similar bifurcation of the Kirkendall marker plane was found in the β-NiAl phase, as shown in Fig. 8.7 in a diffusion couple of $Ni_{41.7}Al_{58.3}/Ni_{72.24}Al_{27.76}$ at 1,000 °C. The optical micrograph in Fig. 8.7b presents the whole interdiffusion zone, and the back scattered electron image in Fig. 8.7c exhibits the position of the two marker planes shown by the presence of ThO_2 particles. One marker plane was found in the Ni-rich and another in the Al-rich side of the β-NiAl phase [11]. To estimate the intrinsic diffusion coefficients over the homogeneity range in this phase, many incremental diffusion couple experiments were conducted such that marker positions are found at different compositions. The composition of the diffusion couples and the annealing times are listed in Table 8.1 along with the couple in which bifurcation of the marker plane was found.

The estimated interdiffusion coefficients and the ratio of the intrinsic diffusion coefficients are shown in Fig. 8.8a and b. From the average of these values, the intrinsic diffusion coefficients are estimated using Eq. 6.66, as shown in Fig. 8.8c. The velocity curve was determined with the help of the concentration gradient

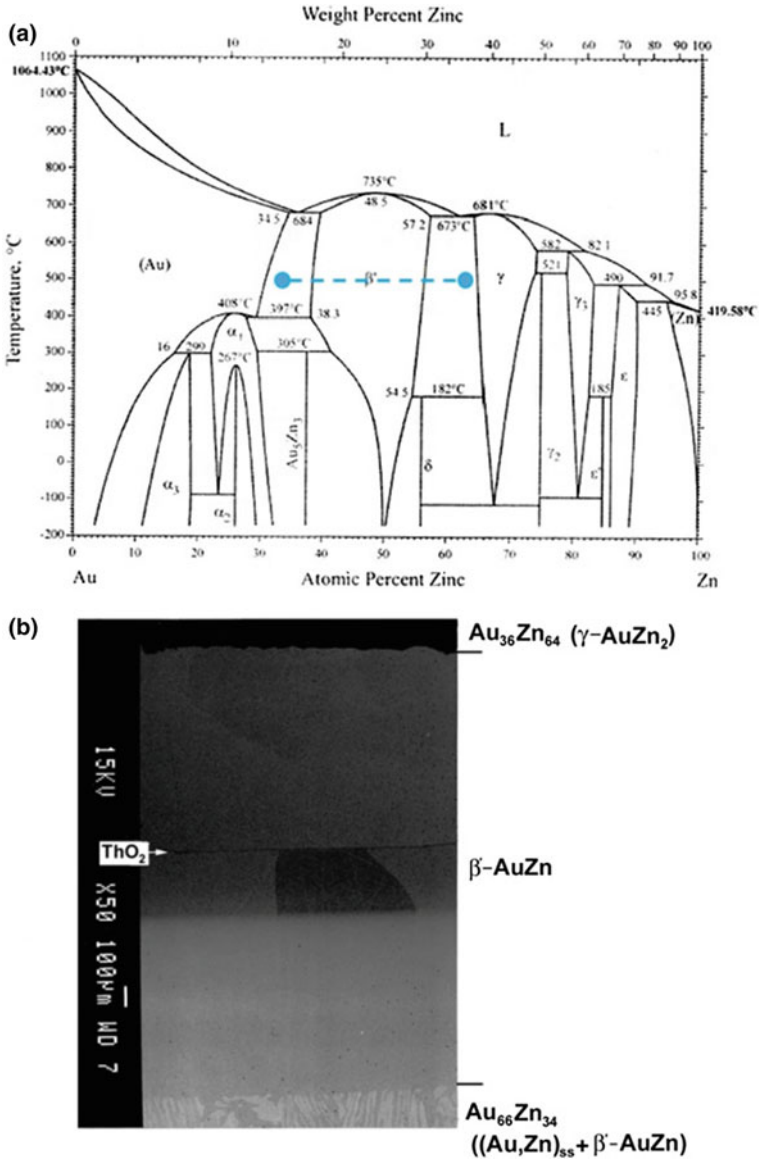

Fig. 8.4 **a** Compositions for a diffusion couple indicating on the Au–Zn phase diagram in which **b** a single marker plane is found [8]

obtained from the measured composition profile in the diffusion couple showing bifurcation of the marker plane, as shown in Fig. 8.9a. Afterward, the straight line determined from $v_K = (x_K - x_o)/2t = x_K/2t$ is drawn by calculating the initial contact plane and from knowledge of the known location of the marker plane. In

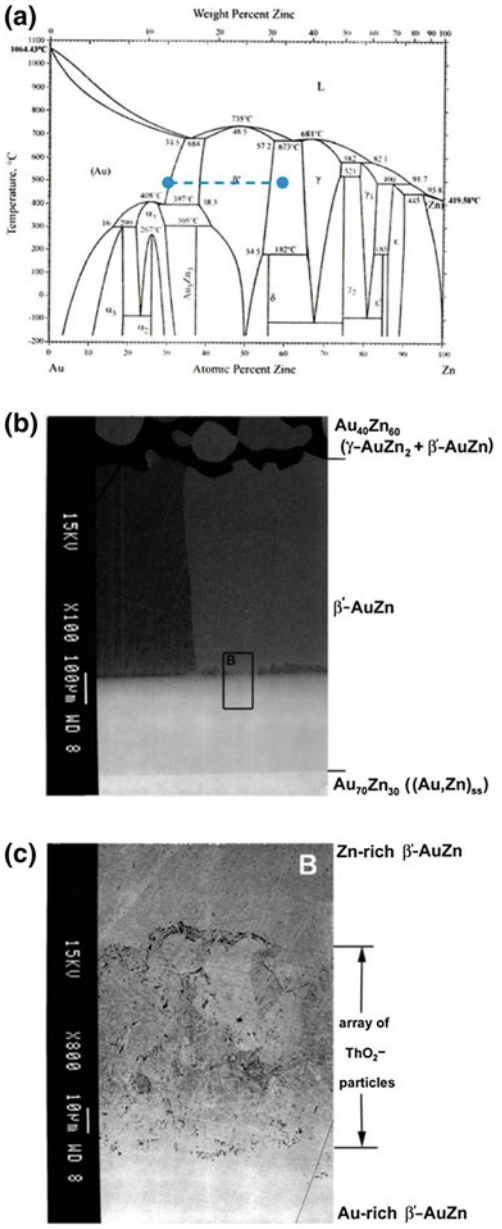

Fig. 8.5 **a** Compositions for a diffusion couple indicating on the Au–Zn phase diagram in which **b** unstable marker plane is found, **c** shows the marker region [8]

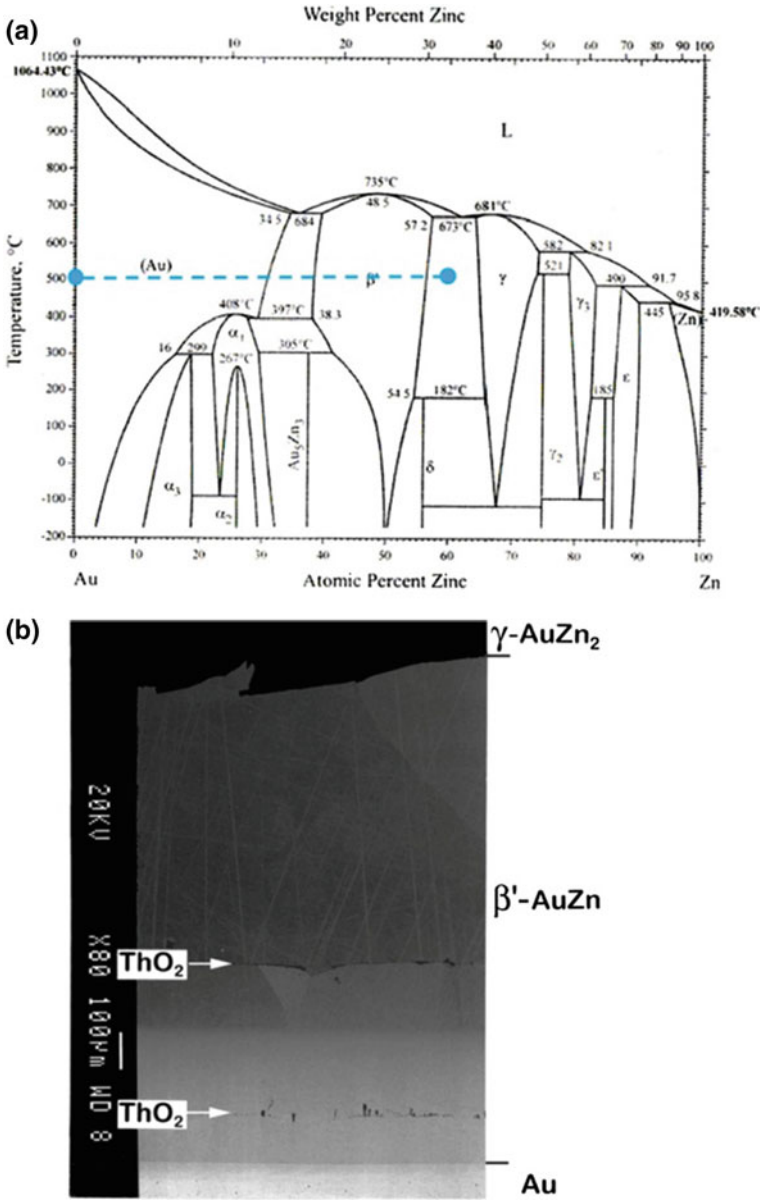

Fig. 8.6 **a** Compositions for a diffusion couple indicating on the Au–Zn phase diagram in which **b** a bifurcation of the marker plane is found [8]

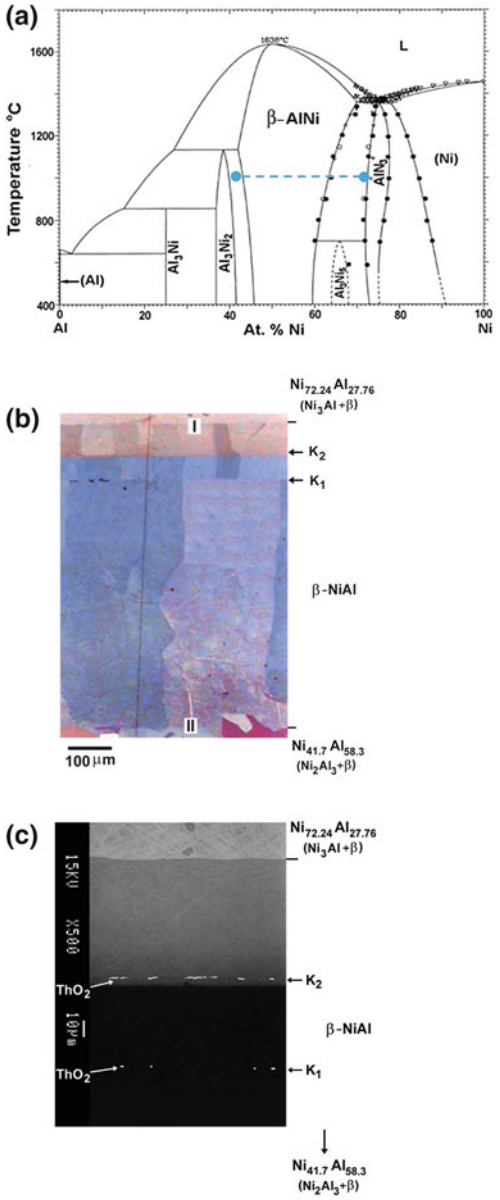

Fig. 8.7 **a** Compositions for a diffusion couple indicating on the Ni–Al phase diagram in which **b** a bifurcation of the marker plane is found in the β-NiAl phase (polarized light microscope image), **c** back scattered electron image clearly shows the location of the marker planes [11]

Table 8.1 Details of the incremental diffusion couple experiments conducted at 1,000 °C are listed

Couple no.	Diffusion couple	Time (h)
1	$Ni_{49.8}Al_{50.2}/Ni_{72.24}Al_{27.76}$	100
2	$Ni_{49.8}Al_{50.2}/Ni_{66.24}Al_{33.76}$	24
3	$Ni_{46}Al_{54}/Ni_{72.24}Al_{27.76}$	24
4	$Ni_{46}Al_{54}/Ni_{66.24}Al_{33.76}$	24
5	$Ni_{46}Al_{54}/Ni_{57.5}Al_{42.5}$	100
6	$Ni_{46}Al_{54}/Ni_{57.5}Al_{42.5}$	24
7	$Ni_{46}Al_{54}/Ni_{49.8}Al_{50.2}$	100
8	$Ni_{49.8}Al_{50.2}/Ni_{57.5}Al_{42.5}$	100
9	$Ni_{46}Al_{54}/Ni_{52.2}Al_{47.8}$	100
10	$Ni_{46}Al_{54}/Ni_{52.2}Al_{47.8}$	24
11	$Ni_{41.7}Al_{58.3}/Ni_{72.24}Al_{27.76}$	24
12	$Ni_{46}Al_{54}/Ni_{54}Al_{46}$	24

the velocity diagram given in Fig. 8.9b, we see that this straight line intersects the velocity curve at two points where it has a negative gradient. There is a jump in the middle of the velocity curve since the composition profile does not grow with any measurable thickness near the stoichiometric composition because of the low interdiffusion coefficients.

The bifurcation of the Kirkendall marker plane shown in the previous examples is found in a single phase. Bifurcation in different phases is found more often than that in a single phase such as in Ag–Zn, Co–Si, Ni–Ti, and Au–Sn systems. The examples for Ag–Zn [12], Co–Si [14, 15], and Ni–Ti [10] systems are shown in Fig. 8.10. In fact, the study on the Ni–Ti system was conducted since this is one of the first systems indicating the likelihood of more than one Kirkendall marker plane. Trifurcation of the Kirkendall marker plane is very rare and it was found in the Ti–Al system [16], which was in fact predicted from the data reported on diffusion parameters before the experimental proof. Theoretically, these behaviors of the marker planes were studied by Höglund and Ågren [17] and Boettinger et al. [18].

8.2 A Physicochemical Approach to Explain the Morphological Evolution in an Interdiffusion Zone

It has been seen in many examples that a characteristic morphology develops in the product phase when grown by reactive diffusion. For example, three incremental diffusion couples in different systems are shown in Fig. 8.11 [14, 15, 19, 20]. It can be seen that a duplex morphology is present whenever there is a Kirkendall marker plane present. In Fig. 8.10a, the bifurcation of the marker plane is shown in the Ag–Zn system [12]. The grain morphologies in different phases are shown in Fig. 8.12. In the ε-$AgZn_3$ and γ-Ag_5Zn_8 phases, the marker planes are

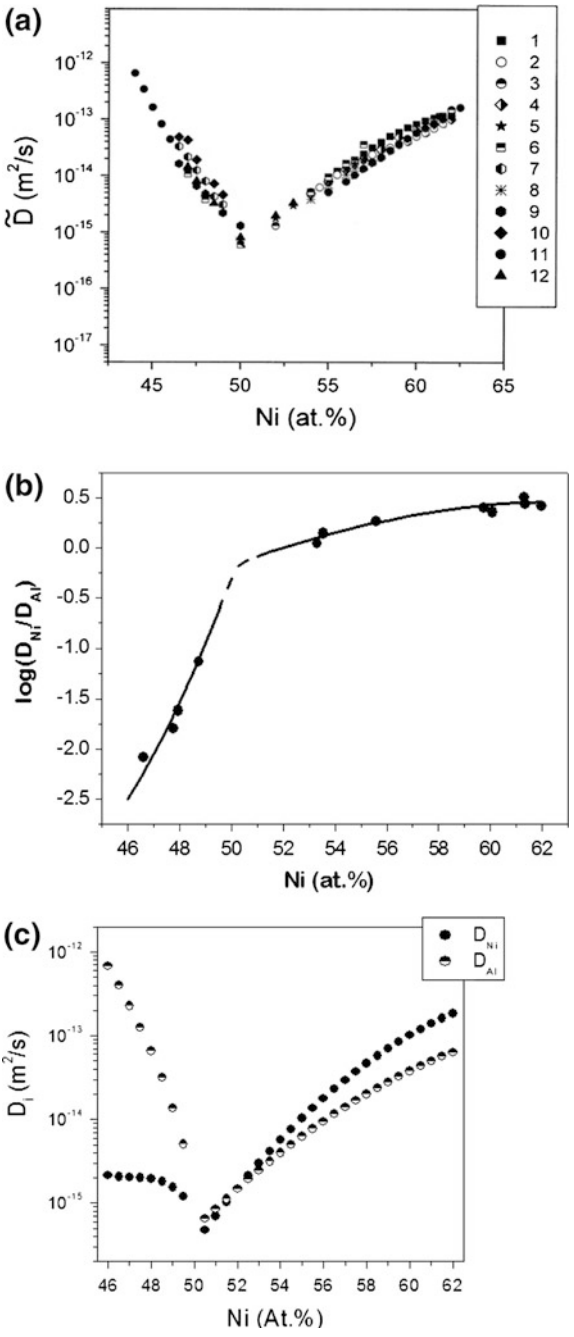

Fig. 8.8 **a** The interdiffusion coefficients, **b** the ratio of the intrinsic diffusion coefficients and **c** the estimated intrinsic diffusion coefficients at different compositions in the β-NiAl phase at 1,000 °C [11]

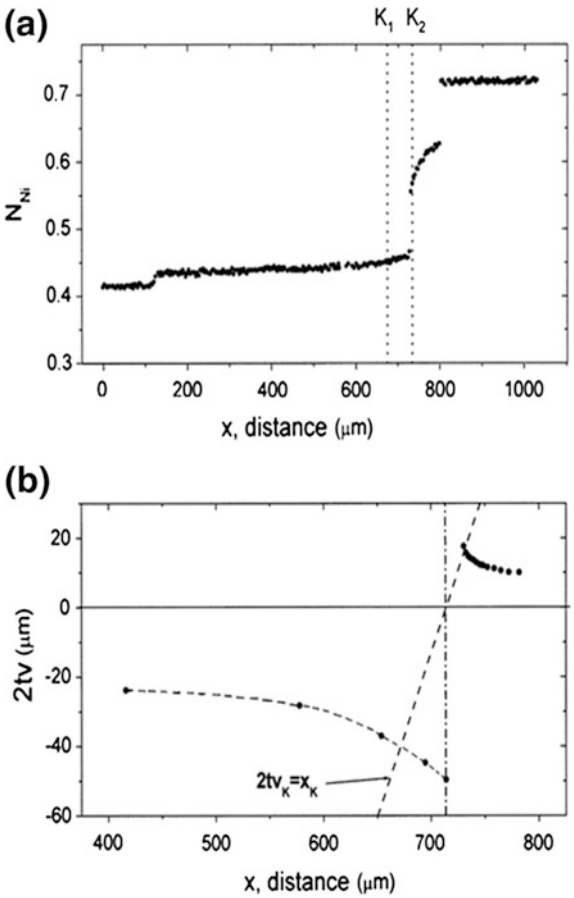

Fig. 8.9 **a** Composition profile and **b** the velocity diagram rationalization of the bifurcation of the marker plane [11]

present and the duplex morphology is also evident. On the other hand, there is no marker plane present in the β-AgZn phase, where uniform and continuous grain morphology is present.

The experimental results shown above indicate that the phase layer grows differently at different interface interphases. In reactive diffusion, the product phase layers are grown because of the reaction/dissociation of the diffusing component from the interfaces. Although the phases are grown by the reactions and/or dissociation at the interface interphases, growth of the phases are not controlled by these processes. We are considering the systems, in which diffusion of components through the phase layers takes longer time to control the growth process. There are many examples, especially in thin-film conditions, where the growth of the phase is reaction controlled, which are not considered here. Before estimating the diffusion parameters with the help of a physicochemical approach,

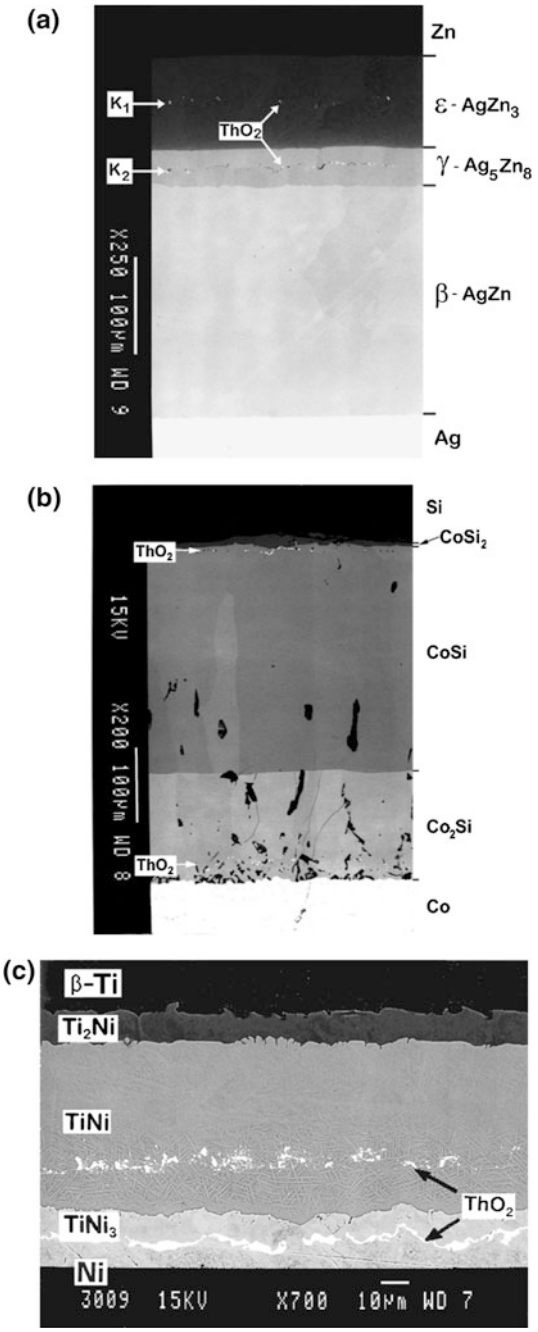

Fig. 8.10 Experimental evidences of bifurcations in **a** Ag–Zn [12], **b** Co–Si [14, 15], and **c** Ni–Ti [10] systems

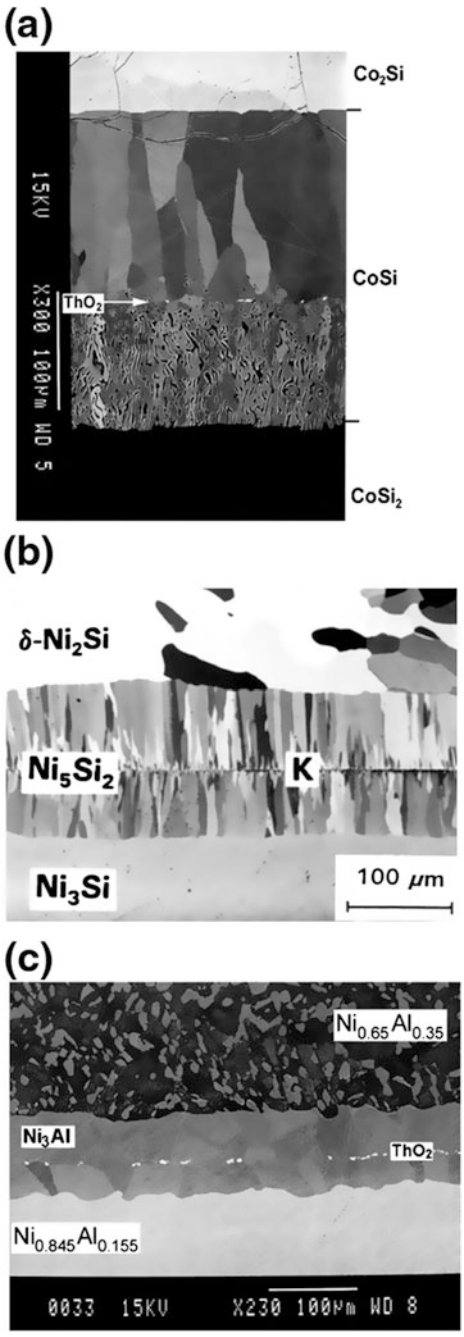

Fig. 8.11 Duplex morphology in the presence of the Kirkendall marker plane in different phases **a** CoSi [14, 15], **b** Ni_5Si_2 [19], and **c** Ni_3Al [20]

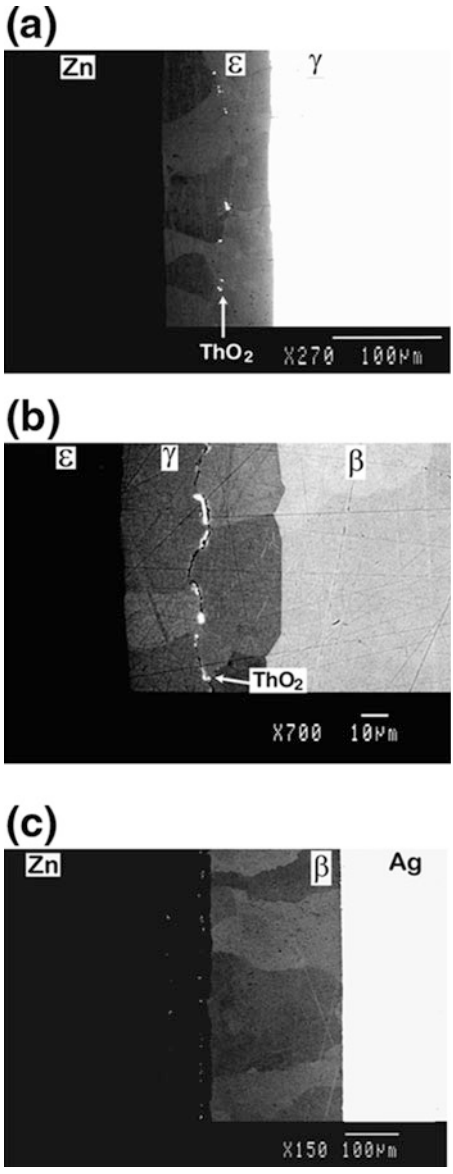

Fig. 8.12 Duplex morphology in the presence of the Kirkendall marker plane in **a** ε-phase, **b** γ-phase and **c** a uniform grain morphology in the β-phase because of the absence of any marker plane [12]

which is developed considering the reactions and dissociations at the interfaces in real systems along with the diffusion of the component through the phase layer, we shall first show that this approach is equivalent to the relations developed in the previous chapters.

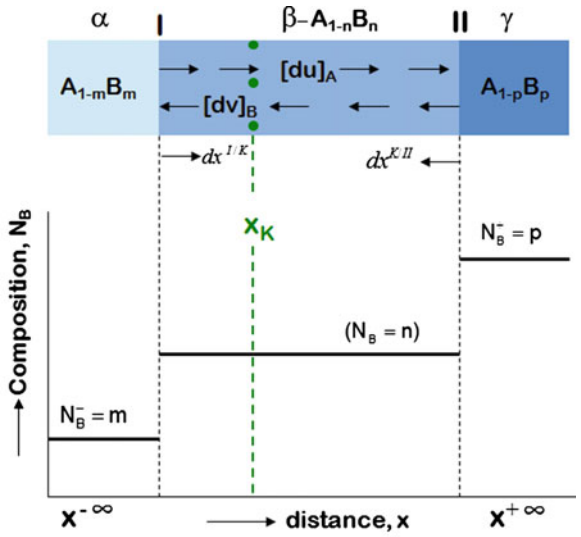

Fig. 8.13 A schematic diagram explaining the physicochemical approach

For the sake of simplicity, let us consider a diffusion couple of α and γ phases in which a line compound β grows in an interdiffusion zone, as shown in Fig. 8.13 [21]. The stoichiometric compositions of the α, β, and γ phases are $A_{1-m}B_m$, $A_{1-n}B_n$, and $A_{1-p}B_p$, respectively. Suppose α is an A-rich and β is a B-rich phase. Therefore, as shown in the figure, A dissociates from the α phase at the interface I to produce the product β phase. The dissociated A then diffuses to the interface II and reacts with the γ phase to produce the β phase. At the same time, B dissociates from the γ phase at the interface II to produce the β phase. The dissociated B diffuses to the interface I to produce the β phase. Therefore, at both interfaces, the product phase β is grown by the dissociation and reaction of the components. Suppose, $[du]_A$ mol/m^2 is the flux of the component A crossing the Kirkendall marker plane in the short period of time dt. Similarly, the flux of the component B that crosses the marker plane in that short period of time is $[dv]_B$ mol/m^2. The location of the marker plane in the interdiffusion zone is shown by filled circles, and the location is denoted as x_K. It is evident that the thickness of the product phase that is grown in the left-hand side of the marker plane is due to the reaction and dissociation at the interface I. On the other hand, the right-hand side of the product phase from the Kirkendall marker plane is grown because of the reaction and dissociation at the interface II. Therefore, we should write the reaction and dissociation equations at the two different interfaces.

Reaction dissociation equations at the interface I:

$$\frac{n}{n-m}du\mathrm{A}_{1-m}\mathrm{B}_m(\alpha\,\text{phase}) \rightarrow du\,[\mathrm{A}]_d + \frac{m}{n-m}du\mathrm{A}_{1-n}\mathrm{B}_n(\beta\,\text{phase})$$

dissociation of A

$$\frac{1-n}{n-m}dv\mathrm{A}_{1-m}\mathrm{B}_m(\alpha\,\text{phase}) + dv\,[\mathrm{B}]_d \rightarrow \frac{1-m}{n-m}dv\mathrm{A}_{1-n}\mathrm{B}_n(\beta\,\text{phase})$$

reaction of B.

Reaction dissociation equations at the interface II:

$$\frac{n}{p-n}du\mathrm{A}_{1-p}\mathrm{B}_p(\gamma\,\text{phase}) + du\,[\mathrm{A}]_d \rightarrow \frac{p}{p-n}du\mathrm{A}_{1-n}\mathrm{B}_n(\beta\,\text{phase})$$

reaction of A

$$\frac{1-n}{p-n}dv\mathrm{A}_{1-p}\mathrm{B}_P(\gamma\,\text{phase}) \rightarrow dv\,[\mathrm{B}]_d + \frac{1-p}{p-n}dv\mathrm{A}_{1-n}\mathrm{B}_n(\beta\,\text{phase})$$

dissociation of A.

The amount of the β phase produced at the interface I is $\frac{1}{n-m}[mdu + (1-m)dv]$ mol/m^2 and at the interface II is $\frac{1}{p-n}[pdu + (1-p)dv]$ mol/m^2. Suppose, the molar volume of the product β phase is v_m, which will be written as v_m^β at latter stage. Suppose, the thicknesses of the phase layer grown from the interfaces I and II in this short period of time dt is $dx^{\mathrm{I/K}}$ and $dx^{\mathrm{K/II}}$, respectively. Therefore, we can write

$$\frac{1}{n-m}[mdu + (1-m)dv]\,v_m = dx^{\mathrm{I/K}} \tag{8.9a}$$

$$\frac{1}{p-n}[pdu + (1-p)dv]\,v_m = dx^{\mathrm{K/II}} \tag{8.9b}$$

Furthermore, we can write both the left- and right-hand sides of the end members, as well as the composition of the product phases as $m = N_{\mathrm{B}}^-$, $p = N_{\mathrm{B}}^+$ and $n = N_{\mathrm{B}}$. Therefore, Eqs. 8.9a and 8.9b can be rewritten as

$$N_{\mathrm{B}}^- du + (1-N_{\mathrm{B}}^-)dv = \frac{N_{\mathrm{B}} - N_{\mathrm{B}}^-}{v_m}dx^{\mathrm{I/K}} \tag{8.10a}$$

$$N_{\mathrm{B}}^+ du + (1-N_{\mathrm{B}}^+)\,dv = \frac{N_{\mathrm{B}}^+ - N_{\mathrm{B}}}{v_m}dx^{\mathrm{K/II}} \tag{8.10b}$$

If the fluxes of the diffusing components A and B are 0 at time $t = 0$ and become u and v after the annealing time t, we can write Eqs. 8.10a and 8.10b by integrating as

$$N_{\mathrm{B}}^{-}\int_{o}^{u} du + (1-N_{\mathrm{B}}^{-})\int_{o}^{v} dv = \int_{x^{-\infty}}^{x_{\mathrm{K}}} \frac{N_{\mathrm{B}}-N_{\mathrm{B}}^{-}}{v_m}dx$$

$$N_{\mathrm{B}}^{-}u + (1-N_{\mathrm{B}}^{-})v = \int_{x^{-\infty}}^{x_{\mathrm{K}}} \frac{N_{\mathrm{B}}-N_{\mathrm{B}}^{-}}{v_m}dx \tag{8.11a}$$

$$N_{\mathrm{B}}^{+}\int_{o}^{u} du + (1-N_{\mathrm{B}}^{+})\int_{o}^{v} dv = \int_{x_{\mathrm{K}}}^{x^{+\infty}} \frac{N_{\mathrm{B}}-N_{\mathrm{B}}^{-}}{v_m}dx$$

$$N_{\mathrm{B}}^{+}u + (1-N_{\mathrm{B}}^{+})v = \int_{x_{\mathrm{K}}}^{x^{+\infty}} \frac{N_{\mathrm{B}}^{+}-N_{\mathrm{B}}}{v_m}dx \tag{8.11b}$$

Now, we would like to write the expressions separately for u and v. Multiplying Eq. 8.11a by $(1-N_{\mathrm{B}}^{+})$ and Eq. 8.11b by $\left(1-N_{\mathrm{B}}^{-}\right)$ and then by subtracting, we get

$$N_{\mathrm{B}}^{-}(1-N_{\mathrm{B}}^{+})u - N_{\mathrm{B}}^{+}(1-N_{\mathrm{B}}^{-})u = (1-N_{\mathrm{B}}^{+})\int_{x^{-\infty}}^{x_{\mathrm{K}}} \frac{N_{\mathrm{B}}-N_{\mathrm{B}}^{-}}{v_m}dx - (1-N_{\mathrm{B}}^{-})\int_{x_{\mathrm{K}}}^{x^{+\infty}} \frac{N_{\mathrm{B}}^{+}-N_{\mathrm{B}}}{v_m}dx$$

$$u = -\left[(1-N_{\mathrm{B}}^{+})\int_{x^{-\infty}}^{x_{\mathrm{K}}} \frac{N_{\mathrm{B}}-N_{\mathrm{B}}^{-}}{N_{\mathrm{B}}^{+}-N_{\mathrm{B}}^{-}}\frac{1}{v_m}dx - (1-N_{\mathrm{B}}^{-})\int_{x_{\mathrm{K}}}^{x^{+\infty}} \frac{N_{\mathrm{B}}^{+}-N_{\mathrm{B}}}{N_{\mathrm{B}}^{+}-N_{\mathrm{B}}^{-}}\frac{1}{v_m}dx\right]$$

Introducing the composition normalizing variable $Y_{\mathrm{B}} = \frac{N_{\mathrm{B}}-N_{\mathrm{B}}^{-}}{N_{\mathrm{B}}^{+}-N_{\mathrm{B}}^{-}}$ such that $1-Y_{\mathrm{B}} = \frac{N_{\mathrm{B}}^{+}-N_{\mathrm{B}}}{N_{\mathrm{B}}^{+}-N_{\mathrm{B}}^{-}}$, we can write

$$\begin{aligned} u &= -\left[(1-N_{\mathrm{B}}^{+})\int_{x^{-\infty}}^{x_{\mathrm{K}}} \frac{Y_{\mathrm{B}}}{v_m}dx - (1-N_{\mathrm{B}}^{-})\int_{x_{\mathrm{K}}}^{x^{+\infty}} \frac{1-Y_{\mathrm{B}}}{v_m}dx\right] \\ u &= -\left[N_{\mathrm{A}}^{+}\int_{x^{-\infty}}^{x_{\mathrm{K}}} \frac{Y_{\mathrm{B}}}{v_m}dx - N_{\mathrm{A}}^{-}\int_{x_{\mathrm{K}}}^{x^{+\infty}} \frac{1-Y_{\mathrm{B}}}{v_m}dx\right] \end{aligned} \tag{8.12a}$$

Multiplying Eq. 8.11a by N_{B}^{-} and Eq. 8.11b by N_{B}^{+} and then by subtracting, we get

$$N_{\mathrm{B}}^{+}(1-N_{\mathrm{B}}^{-})v\ -N_{\mathrm{B}}^{-}(1-N_{\mathrm{B}}^{+})v=N_{\mathrm{B}}^{+}\int_{x^{-\infty}}^{x_{\mathrm{K}}}\frac{N_{\mathrm{B}}-N_{\mathrm{B}}^{-}}{v_m}dx-N_{\mathrm{B}}^{-}\int_{x_{\mathrm{K}}}^{x^{+\infty}}\frac{N_{\mathrm{B}}^{+}-N_{\mathrm{B}}}{v_m}dx$$

$$v=N_{\mathrm{B}}^{+}\int_{x^{-\infty}}^{x_{\mathrm{K}}}\frac{N_{\mathrm{B}}-N_{\mathrm{B}}^{-}}{N_{\mathrm{B}}^{+}-N_{\mathrm{B}}^{-}}\frac{1}{v_m}dx-N_{\mathrm{B}}^{-}\int_{x_{\mathrm{K}}}^{x^{+\infty}}\frac{N_{\mathrm{B}}^{+}-N_{\mathrm{B}}}{N_{\mathrm{B}}^{+}-N_{\mathrm{B}}^{-}}\frac{1}{v_m}dx$$

$$v=N_{\mathrm{B}}^{+}\int_{x^{-\infty}}^{x_{\mathrm{K}}}\frac{Y_{\mathrm{B}}}{v_m}dx-N_{\mathrm{B}}^{-}\int_{x_{\mathrm{K}}}^{x^{+\infty}}\frac{1-Y_{\mathrm{B}}}{v_m}dx \tag{8.12b}$$

The intrinsic flux of A that is J_{A} and the intrinsic flux of B that is J_{B} can be related to u and v. It is a fact that the intrinsic fluxes are inversely proportional to $t^{1/2}$. Moreover, the sign of the flux of A should be taken as positive since it diffuses from left to right and the flux of B should be taken as negative since it diffuses from right to left. Therefore, we can write

$$u=\int_0^u du=\int_0^t J_{\mathrm{A}}\,dt=\int_0^t\frac{k}{t^{1/2}}dt=\frac{kt^{1/2}}{1/2}=2tJ_{\mathrm{A}}=-2tD_{\mathrm{A}}\frac{\partial C_{\mathrm{A}}}{\partial x} \tag{8.13a}$$

$$v=\int_0^v dv=-\int_0^t J_{\mathrm{B}}\,dt=-\int_0^t\frac{k}{t^{1/2}}dt=-2tJ_{\mathrm{B}}=2tD_{\mathrm{B}}\frac{\partial C_{\mathrm{B}}}{\partial x} \tag{8.13b}$$

where k is the proportionality constant. Note here that $J_i=-D_i\frac{\partial C_i}{\partial x}$. From Eqs. 8.12 and 8.13a, we can write

$$D_{\mathrm{A}}=\frac{1}{2t}\left(\frac{\partial x}{\partial C_{\mathrm{A}}}\right)\left[N_{\mathrm{A}}^{+}\int_{x^{-\infty}}^{x_{\mathrm{K}}}\frac{Y}{v_m}dx-N_{\mathrm{A}}^{-}\int_{x_{\mathrm{K}}}^{x^{+\infty}}\frac{1-Y}{v_m}dx\right] \tag{8.14a}$$

$$D_{\mathrm{B}}=\frac{1}{2t}\left(\frac{\partial x}{\partial C_{\mathrm{B}}}\right)\left[N_{\mathrm{B}}^{+}\int_{x^{-\infty}}^{x_{\mathrm{K}}}\frac{Y}{v_m}dx-N_{\mathrm{B}}^{-}\int_{x_{\mathrm{K}}}^{x^{+\infty}}\frac{1-Y}{v_m}dx\right] \tag{8.14b}$$

Note that these are the relations developed by van Loo [22] and are those that we derived earlier in Chap. 6 following the approach by Wagner [13]. From the standard thermodynamic relations $\partial C_A=\left(\bar{v}_B/v_m^2\right)\partial N_A$, $\partial C_B=\left(\bar{v}_A/v_m^2\right)\partial N_B$ (Eq. 1.150), we can write the ratio of the intrinsic diffusion coefficients as

$$\frac{\bar{v}_A D_B}{\bar{v}_B D_A} = \frac{J_B}{J_A} = \frac{v}{u} \tag{8.15a}$$

Following Eq. 6.91, we can write this with respect to the ratio of the tracer diffusion coefficients as

$$\frac{D_B^*}{D_A^*} = \frac{\bar{v}_A D_B}{\bar{v}_B D_A} = \frac{J_B}{J_A} = \frac{v}{u} \tag{8.15b}$$

Therefore, since the partial molar volumes are not known in a phase with a narrow homogeneity range, we actually measure the ratio of the tracer diffusion coefficients after neglecting the role of the vacancy wind effect, as explained in Chap. 6.

Previously in Chap. 6, we derived the relation between the interdiffusion coefficients and the intrinsic diffusion coefficients as

$$\tilde{D} = C_A \bar{v}_A D_B + C_B \bar{v}_B D_A \tag{8.16}$$

since $N_B + N_A = 1$, $C_i = \frac{N_i}{v_m}$, we can write the interdiffusion coefficients with respect to u and v with the help of Eqs. 8.13a and 8.13b as [21]

$$\tilde{D} = \frac{v_m}{2t} \frac{\partial x}{\partial N_B} [N_B u + N_A v] \tag{8.17}$$

In the case of a compound with a very narrow homogeneity range, since we cannot measure the composition profile, the integrated diffusion coefficient is measured. With respect to u and v, we can express this as [23]

$$\tilde{D}_{\text{int}}^{\beta} = \int_{N_B^I}^{N_B^{II}} \tilde{D}\, dN_B = \int_{x_\beta^I}^{x_\beta^{II}} \frac{v_m}{2t} [N_B u + N_A v]\, dx = \frac{v_m^\beta}{2t} \left[N_B^\beta u + N_A^\beta v \right] \Delta x_\beta \tag{8.18}$$

As explained in Chap. 6, here the unknown composition range of the β phase is $N_B^{II} - N_B^I$, the thickness of the phase layer is $\Delta x_\beta = x_\beta^{II} - x_\beta^I$. The average molar volume of the phase v_m^β and the composition N_B^β can be considered as constant and during a fixed annealing time of t fixed amount of fluxes, u and v transfer through the Kirkendall marker plane. The values of u and v can be estimated from the composition profile using the relations expressed in Eqs. 8.12a and 8.12b. It should be noted here that by replacing these relations in Eqs. 8.17 and 8.18, we can derive the same relations for the interdiffusion coefficient and the integrated diffusion coefficient as derived by Wagner, which are described in Chaps. 6 and 7.

The velocity of the marker plane following Eq. 6.62 can be estimated by

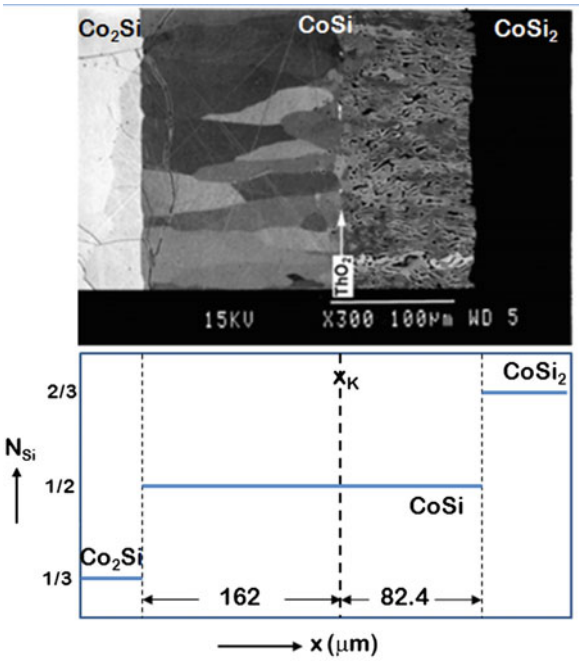

Fig. 8.14 Interdiffusion zone of the CoSi phase in a diffusion couple of Co_2Si/$CoSi_2$ annealed at 1,000 °C for 49 h and use of the physicochemical approach for the estimation of the diffusion parameter [14]

$$v_K = -(\bar{v}_A J_A + \bar{v}_B J_B)$$

Replacing Eq. 8.13a in the above equation, we get

$$v_K = -\left(\bar{v}_A \frac{u}{2t} - \bar{v}_B \frac{v}{2t}\right) = \frac{1}{2t}(\bar{v}_B v - \bar{v}_A u) \tag{8.19a}$$

If the values of the partial molar volumes are not known—for instance, in a phase with a narrow homogeneity range—we consider $v_m = \bar{v}_A = \bar{v}_B$, where v_m is the molar volume of the product phase. Therefore, we can write

$$x_K = 2tv_K = v_m(v - u) \tag{8.19b}$$

It can be understood from the above discussion that the phase layer grows differently from the two different interfaces and we should expect a duplex morphology separated by a Kirkendall marker plane as shown in Fig. 8.11. Therefore, one expects the same values of diffusion coefficients when derived following different approaches explained in Chaps. 6 and 7 or this chapter. The physicochemical approach has an additional benefit that it sheds light on the morphological evolutions in the interdiffusion zone.

8.3 The Application of the Physicochemical Approach in an Incremental Diffusion Couple with a Single Product Phase

Let us now apply this physicochemical approach to estimate the integrated diffusion coefficient and the ratio of the tracer diffusion coefficients in real systems. We consider the growth of CoSi in a diffusion couple of Co_2Si and $CoSi_2$ annealed at 1,100 °C for 49 h, as shown in Fig. 8.11a. The description of the analysis is presented in Fig. 8.14 [16, 21]. It is to be anticipated that Co will dissociate from the Co-rich phase Co_2Si at the interface I to produce the CoSi product phase. Co will then diffuse to the interface II to react with the $CoSi_2$ phase and produce the CoSi phase. Similarly, Si dissociates from the Si-rich phase (the $CoSi_2$ phase at the interface II) to produce the CoSi phase. The dissociated Si diffuses to the interface I to react with the Co_2Si phase and produce the CoSi phase.

In terms of chemical reaction equations:

At the interface I (Co_2Si/CoSi)

$$3u\mathrm{Co}_{2/3}\mathrm{Si}_{1/3} \rightarrow [u]_{\mathrm{Co}} + 2u\mathrm{Co}_{1/2}\mathrm{Si}_{1/2}$$
$$3v\mathrm{Co}_{2/3}\mathrm{Si}_{1/3} + [v]_{\mathrm{Si}} \rightarrow 4v\mathrm{Co}_{1/2}\mathrm{Si}_{1/2}$$

At the interface II (CoSi/$CoSi_2$)

$$3u\mathrm{Co}_{1/3}\mathrm{Si}_{2/3} + [u]_{\mathrm{Co}} \rightarrow 4u\mathrm{Co}_{1/2}\mathrm{Si}_{1/2}$$
$$3v\mathrm{Co}_{1/3}\mathrm{Si}_{2/3} \rightarrow [v]_{\mathrm{Si}} + 2v\mathrm{Co}_{1/2}\mathrm{Si}_{1/2}$$

The parameters $[u]_{\mathrm{Co}}$ and $[v]_{\mathrm{Si}}$ are the number of moles of Co and Si atoms, respectively, transferred per unit area of the reaction layer during the total diffusion time. Following on from this, we can write

$$(2u + 4v)\, v_m^{\mathrm{CoSi}} = \Delta x_{\mathrm{CoSi}}^{\mathrm{I}} \tag{8.20a}$$

$$(4u + 2v)\, v_m^{\mathrm{CoSi}} = \Delta x_{\mathrm{CoSi}}^{\mathrm{II}} \tag{8.20b}$$

Note that the same relations can be obtained directly from Eq. 8.11.

$$N_{\mathrm{Si}}^{-}u + \left(1 - N_{\mathrm{Si}}^{-}\right)v = \int_{x^{-\infty}}^{x_{\mathrm{K}}} \frac{N_{\mathrm{Si}} - N_{\mathrm{Si}}^{-}}{v_m^{\mathrm{CoSi}}}\, dx = \frac{N_{\mathrm{Si}} - N_{\mathrm{Si}}^{-}}{v_m^{\mathrm{CoSi}}} \int_{x^{-\infty}}^{x_{\mathrm{K}}} dx = \frac{N_{\mathrm{Si}} - N_{\mathrm{Si}}^{-}}{v_m^{\mathrm{CoSi}}} \Delta x_{\mathrm{CoSi}}^{\mathrm{I}}$$

$$N_{\mathrm{Si}}^{+}u + \left(1 - N_{\mathrm{Si}}^{+}\right)v = \int_{x_{\mathrm{K}}}^{x^{+\infty}} \frac{N_{\mathrm{Si}}^{+} - N_{\mathrm{Si}}}{v_m^{\mathrm{CoSi}}}\, dx = \frac{N_{\mathrm{Si}}^{+} - N_{\mathrm{Si}}}{v_m^{\mathrm{CoSi}}} \int_{x_{\mathrm{K}}}^{x^{+\infty}} dx = \frac{N_{\mathrm{Si}}^{+} - N_{\mathrm{Si}}}{v_m^{\mathrm{CoSi}}} \Delta x_{\mathrm{CoSi}}^{\mathrm{II}}$$

In this example, $N_{\mathrm{Si}}^{-} = 1/3$, $1 - N_{\mathrm{Si}}^{-} = 2/3$, $N_{\mathrm{Si}}^{+} = 2/3$, $1 - N_{\mathrm{Si}}^{+} = 1/3$, $N_{\mathrm{Si}} = 1/2$ and $1 - N_{Si} = 1/2$. We are considering a phase with a narrow composition range that is an average composition and the constant molar volume of the phase. It can be seen that from the composition values written above, we get the same relations in Eq. 8.20.

The thicknesses of the sublayers measured from the microstructure shown in Fig. 8.14 are $\Delta x_{\mathrm{CoSi}}^{\mathrm{I}} = 162\ \mu\mathrm{m}$. Note here that the actual length of $\Delta x_{\mathrm{CoSi}}^{\mathrm{II}}$ is measured as 107 μm (approximately 23 %); however, the length of $\Delta x_{\mathrm{CoSi}}^{\mathrm{II}} = 82.4\ \mu\mathrm{m}$ is considered for the calculation because of the presence of pores in this sublayer [14, 15]. The molar volume of the CoSi phase is $v_m^{\mathrm{CoSi}} = 6.6 \times 10^{-6}\ \mathrm{m^3/mol}$. Using these values, we find $u = 0.07$ and $v = 6.1\ \mathrm{mol/m^2}$. Therefore, the integrated diffusion coefficient and the ratio of the tracer diffusion coefficients can be estimated using the relations expressed in Eqs. 7.15b and 7.18 as (for an annealing time of 49 h)

$$\frac{D_{\mathrm{Si}}^{*}}{D_{\mathrm{Co}}^{*}} = \frac{v}{u} = 87$$

$$\begin{aligned}\tilde{D}_{\mathrm{int}}^{\mathrm{CoSi}} &= \frac{v_m^{\mathrm{CoSi}}}{2t}\left[N_{\mathrm{Si}}^{\mathrm{CoSi}}u + N_{\mathrm{Co}}^{\mathrm{CoSi}}v\right]\Delta x_{\beta} \\ &= \frac{6.60 \times 10^{-6}}{2 \times 49 \times 60 \times 60}\left[\frac{1}{2} \times 0.07 + \frac{1}{2} \times 6.1\right](162 + 82.4) \times 10^{-6} \\ &= 1.41 \times 10^{-14}\ \mathrm{m^2/s}\end{aligned}$$

Once again, it was possible to calculate the same values using the relations shown in Chap. 7 (Eq. 7.15).

$$\begin{aligned}\tilde{D}_{\mathrm{int}}^{\mathrm{CoSi}} &= \frac{\left(N_{\mathrm{Si}}^{\mathrm{CoSi}} - N_{\mathrm{Si}}^{\mathrm{Co_2Si}}\right)\left(N_{\mathrm{Si}}^{\mathrm{CoSi_2}} - N_{\mathrm{Si}}^{\mathrm{CoSi}}\right)}{\left(N_{\mathrm{Si}}^{\mathrm{CoSi_2}} - N_{\mathrm{Si}}^{\mathrm{Co_2Si}}\right)}\frac{\Delta x_{\mathrm{CoSi}}^{2}}{2t} \\ &= \frac{1/6 \times 1/6}{1/3} \times \frac{(162 + 82.4) \times 10^{-6}}{2 \times 49 \times 60 \times 60} \\ &= 1.41 \times 10^{-14}\ \mathrm{m^2/s}\end{aligned}$$

Now, let us consider an incremental couple in which a single product phase grows from the end members with two phase alloys, as shown in Fig. 8.15 [23]. One of the end members has a composition of $Co_{0.81}Si_{0.19}$. It can be observed from the phase diagram and the alloy in the end member that it is a phase mixture of ε-Co—that is, ε-Co(Si) solid solution with a composition of $Co_{0.83}Si_{0.17}$ at 1,100 °C. Another alloy used as an end member has an average composition of $Co_{0.52}Si_{0.48}$, meaning that it is a phase mixture of Co_2Si and CoSi phases. The volume fraction of the phases can be estimated by the lever rule, as explained in Chap. 1.

Before proceeding to the reaction equations, it is necessary to understand the mechanism by which the product phase grows at the interdiffusion zone. Note that

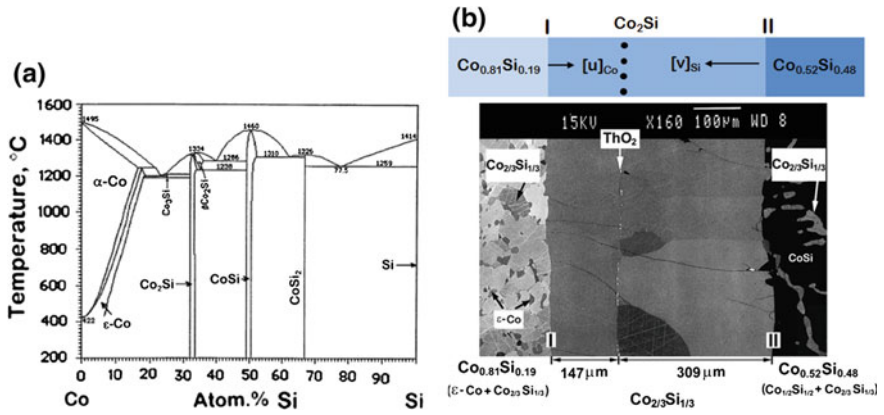

Fig. 8.15 **a** Co–Si phase diagram and **b** use of the physicochemical approach in the Co_2Si phase grown at 1,100 °C after annealing for 100 h [23]

only the ε-Co(Si) phase from the left-hand side end member and the CoSi phase from the right-hand side end member will take part in the reaction or the dissociation process. The Co_2Si phase that is already present in the alloy will directly add to the product phase. This is the reason, as explained in Chap. 7 (Sect. 7.4), the growth rate of a product phase is different depending on the end-member compositions. If we select alloys having a composition closer to the product phase, the growth kinetics of the phase will be higher since the amount of this phase—which can be directly added to the product phase—is higher. The reaction dissociation equations at the interfaces can be written as [23].

At the interface I ($Co_{0.81}Si_{0.19}/Co_2Si$)

$$2.04u\mathrm{Co}_{0.83}\mathrm{Si}_{0.17}(\varepsilon) \rightarrow [u]_{\mathrm{Co}} + 1.04u\mathrm{Co}_{2/3}\mathrm{Si}_{1/3}$$
$$4.06v\mathrm{Co}_{0.83}\mathrm{Si}_{0.17}(\varepsilon) + [v]_{\mathrm{Si}} \rightarrow 5.06v\mathrm{Co}_{2/3}\mathrm{Si}_{1/3}$$

At the interface II ($CoSi/CoSi_2$)

$$2u\mathrm{Co}_{1/2}\mathrm{Si}_{1/2} + [u]_{\mathrm{Co}} \rightarrow 3u\mathrm{Co}_{2/3}\mathrm{Si}_{1/3}$$
$$4v\mathrm{Co}_{1/2}\mathrm{Si}_{1/2} \rightarrow [v]_{\mathrm{Si}} + 3v\mathrm{Co}_{2/3}\mathrm{Si}_{1/3}$$

The parameters $[u]_{\mathrm{Co}}$ and $[v]_{\mathrm{Si}}$ are the number of moles of Co and Si atoms, respectively, transferred per unit area of the reaction layer during the total diffusion time. Therefore, $(1.04u + 5.06v)$ moles of the Co_2Si phase are produced at the interface I caused by the dissociation and reaction processes. Moreover, as already discussed for the $(2.04u + 4.06v)$ moles of the ε-Co(Si) phase that is consumed at the interface I, a portion of the Co_2Si phase will be directly added to the product phase. Following the lever rule, we know that in an alloy with an average composition of $Co_{0.81}Si_{0.19}$, the ratio of the mole fractions of the Co_2Si

phase to the ε-Co(Si) phase with a composition of $Co_{0.83}Si_{0.17}$ is $\frac{0.19-0.17}{1/3-0.19} = 0.14$. For the consumption of $(2.04u + 4.06v)$ moles of the ε-Co(Si) phase at this interface, $0.14(2.04u + 4.06v)$ moles of the Co_2Si phase will be directly added to the product phase. Therefore, the growth of the Co_2Si phase from the interface I can be written as

$$\begin{aligned}&[(1.04u + 5.06v) + 0.14(2.04u + 4.06v)]v_{\mathrm{m}}^{\mathrm{Co_2Si}} = \Delta x^{I}_{Co_2Si}\\&(1.3u + 5.6v)v_{\mathrm{m}}^{\mathrm{Co_2Si}} = \Delta x^{I}_{Co_2Si}\end{aligned} \tag{8.21a}$$

Similarly, at the interface II, $(3u + 3v)$ moles of the Co_2Si phase are produced by the reaction and dissociation processes. Since $(2u + 4v)$ moles of CoSi are consumed at this interface, a portion of the Co_2Si phase will be directly added to the product phase. Following the lever rule, the ratio of moles of the Co_2Si phase to the CoSi phase in an alloy with an average composition of a $Co_{0.52}Si_{0.48}$ alloy is $\frac{0.5-0.48}{0.48-1/3} = 0.136$. For the consumption of $(2u + 4v)$ moles of CoSi, $0.136(2u + 4v)$ moles of the Co_2Si phase will be directly added to the product phase. Therefore, the growth of the Co_2Si phase from the interface II can be written as

$$\begin{aligned}&[(3u + 3v) + 0.136(2u + 4v)]v_{\mathrm{m}}^{\mathrm{Co_2Si}} = \Delta x^{II}_{Co_2Si}\\&(3.3u + 3.5v)v_{\mathrm{m}}^{\mathrm{Co_2Si}} = \Delta x^{II}_{Co_2Si}\end{aligned} \tag{8.21b}$$

The same relations can be obtained directly from Eq. 8.11.

$$N_{\mathrm{Si}}^{-}u + (1 - N_{\mathrm{Si}}^{-})v = \int_{x^{-\infty}}^{x_{\mathrm{K}}} \frac{N_{\mathrm{Si}} - N_{\mathrm{Si}}^{-}}{v_m^{\mathrm{Co_2Si}}}dx = \frac{N_{\mathrm{Si}} - N_{\mathrm{Si}}^{-}}{v_m^{\mathrm{Co_2Si}}}\int_{x^{-\infty}}^{x_{\mathrm{K}}} dx = \frac{N_{\mathrm{Si}} - N_{\mathrm{Si}}^{-}}{v_m^{\mathrm{Co_2Si}}}\Delta x^{\mathrm{I}}_{\mathrm{Co_2Si}}$$

$$N_{\mathrm{Si}}^{+}u + (1 - N_{\mathrm{Si}}^{+})v = \int_{x_{\mathrm{K}}}^{x^{+\infty}} \frac{N_{\mathrm{Si}}^{+} - N_{\mathrm{Si}}}{v_m^{\mathrm{Co_2Si}}}dx = \frac{N_{\mathrm{Si}}^{+} - N_{\mathrm{Si}}}{v_m^{\mathrm{Co_2Si}}}\int_{x_{\mathrm{K}}}^{x^{+\infty}} dx = \frac{N_{\mathrm{Si}}^{+} - N_{\mathrm{Si}}}{v_m^{\mathrm{Co_2Si}}}\Delta x^{\mathrm{II}}_{\mathrm{Co_2Si}}$$

In this example, $N_{\mathrm{Si}}^{-} = 0.19$, $1 - N_{\mathrm{Si}}^{-} = 0.81$, $N_{\mathrm{Si}}^{+} = 0.48$, $1 - N_{\mathrm{Si}}^{+} = 0.52$, $N_{\mathrm{Si}} = 1/3$ and $1 - N_{\mathrm{Si}} = 2/3$. It can be seen that from the composition values written above, we arrive at the same relations as those in Eq. 8.21.

The thicknesses of the sublayers measured from the microstructure shown in Fig. 8.15 are $\Delta x^{\mathrm{I}}_{\mathrm{Co_2Si}} = 147\,\mu\mathrm{m}$ and $\Delta x^{\mathrm{II}}_{\mathrm{Co_2Si}} = 309\,\mu\mathrm{m}$. The molar volume of the Co_2Si phase is $v_m^{\mathrm{Co_2Si}} = 6.56 \times 10^{-6}\ \mathrm{m^3/mol}$. Using these values, we find $u = 13.55$ and $v = 0.78$. Therefore, the integrated diffusion coefficient and the ratio of the tracer diffusion coefficients can be estimated using the relations expressed in Eqs. 8.15b and 8.18 as (for an annealing time of 100 h)

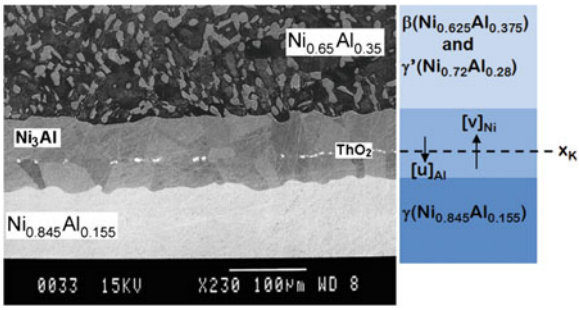

Fig. 8.16 Use of the physicochemical approach in Ni_3Al phase grown in a diffusion couple at 1,000 °C annealed for 196 h [20]

$$\frac{D^*_{Si}}{D^*_{Co}} = \frac{v}{u} = 0.06$$

$$\tilde{D}^{Co_2Si}_{int} = \frac{v_m^{Co_2Si}}{2t}\left[N_{Si}^{Co_2Si}u + N_{Co}^{Co_2Si}v\right]\Delta x_{Co_2Si}$$

$$= \frac{6.56\times10^{-6}}{2\times100\times60\times60}\left[\frac{1}{3}\times13.55+\frac{2}{3}\times0.78\right](147+309)\times10^{-6}$$

$$= 2.1\times10^{-14}\,m^2/s$$

It should be pointed out here that the relations developed in this chapter could also be used to calculate the diffusion parameters at the Kirkendall marker plane where the composition varies in the interdiffusion zone. For example, as shown in Fig. 8.16 in a $Ni_{0.65}Al_{0.35}/Ni_{0.845}Al_{0.155}$ diffusion couple, the γ' phase grows in the interdiffusion zone [21]. It can be understood from the Ni–Al phase diagram in Fig. 4.11a [24] that $Ni_{0.65}Al_{0.35}$ is a phase mixture of the β-NiAl phase with the composition of the $Ni_{0.625}Al_{0.375}$ (dark matrix) and the γ'-Ni_3Al phase (gray precipitates) having the composition of $Ni_{0.72}Al_{0.28}$. The other end member with a composition of $Ni_{0.845}Al_{0.155}$ is a γ-Ni(Al) solid-solution phase [20]. Unlike the previous examples, in this case, there will be composition redistribution after the γ' phase gets added to the product phase from the end member.

The composition profile of the interdiffusion zone is shown in Fig. 8.17a. We consider that u and v in mol/m^2 are the fluxes of Al and Ni crossing the Kirkendall marker plane for the total annealing time of 196 h. The relations expressed in Eq. 8.11 for this diffusion couple can be written as

$$0.65u + 0.35v = \int_{x^{-\infty}}^{x_K} \frac{N_{Ni} - 0.65}{v_m}\,dx \tag{8.22a}$$

$$0.845u + 0.155v = \int_{x_K}^{x^{+\infty}} \frac{0.845 - N_{Ni}}{v_m}\,dx \tag{8.22b}$$

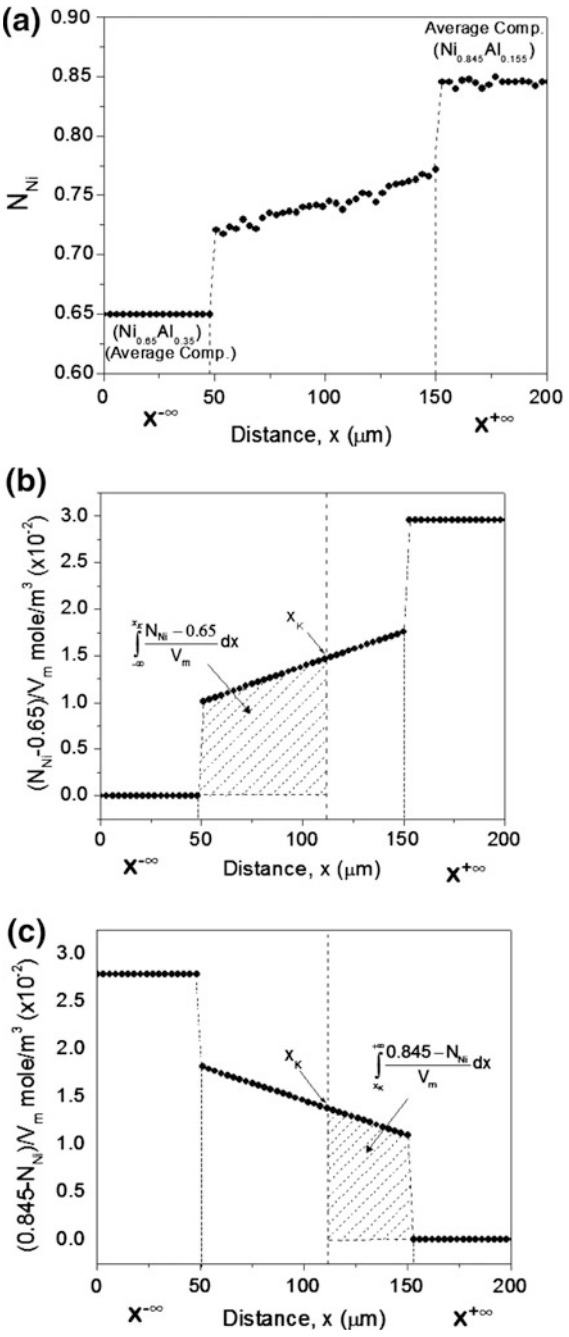

Fig. 8.17 Explanation of estimation of the diffusion parameters by physicochemical approach in Ni_3Al [21]

Note here that $N_B^- = 0.65$, $1 - N_B^- = 0.35$, $N_B^+ = 0.845$ and $1 - N_B^+ = 0.155$. The $(N_{Ni} - 0.65)/v_m$ versus x and $(0.845 - N_{Ni})/v_m$ versus x plots are given in Fig. 8.17b and c, respectively, to determine the values of u and v. The variation in the molar volume of the Ni_3Al phase with composition is available in published work as [20]

$$v_m = 6.60 + 0.823(1 - N_{Ni}) + 0.965\left(1 - N_{Ni}\right)^2 \tag{8.22c}$$

The partial molar volumes of Ni and Al from Eq. 8.22c are estimated as 6.54×10^{-6} and 7.85×10^{-6} m^3/mol.

The values under integral are determined graphically from Fig. 8.17b and c and the values of u and v using Eq. 8.22 are found to be 0.28 and 1.67 mol/m^2, respectively. The slope $d(N_{Ni}/v_m)/dx$ is found to be 7.49×10^7 mol/m^4. Following, the values of the intrinsic diffusion coefficients of the component are estimated as $D_{Ni} = 1.58 \times 10^{-14}$ and $D_{Al} = 3.2 \times 10^{-15}$ m^2/s.

8.4 The Application of the Physicochemical Approach to Explain the Multiphase Growth

The diffusion process for multiphase growth is highly complicated in comparison with the growth of a single phase in an interdiffusion zone. Instead of considering the calculated diffusion parameters from a single composition profile, we shall use the diffusion parameters estimated from the incremental diffusion couples to explain the morphological evolution during multiphase growth. Since there is an extensive data available for the Co–Si system, we shall consider this. A similar method can be used in the other systems once the diffusion process is understood in this system. The useful data at 1,100 °C are listed in Table 8.2 [16]. We consider a diffusion couple of Co/$CoSi_2$, in which, according to the phase diagram shown in Fig. 8.15a, two phases (Co_2Si and CoSi) should grow in the interdiffusion zone. Such a schematic diffusion couple is shown in Fig. 8.18. As shown in this figure, it is necessary to consider a Kirkendall marker plane in both the phases. Following, we consider that the total flux of Co and Si that crosses the Kirkendall marker plane in the Co_2Si phase is $[m]_{Co}$ and $[n]_{Si}$, respectively. Similarly, the total flux of Co and Si that crosses the Kirkendall marker plane in the CoSi phase is $[p]_{Co}$ and $[q]_{Si}$, respectively. The growth of the Co_2Si phase at the interface I occurs by the reaction of Co with the Si-diffused component through this phase after the dissociation at the interface II. At the interface II, the same phase grows because of the dissociation of Si from the CoSi phase. At the same time, the phase also grows because of the reaction between CoSi and Co that diffuses from the interface I. At the same time, the CoSi phase grows at the interface II because of the dissociation of Co from the Co_2Si phase and the reaction of Si with the same phase. The dissociated Co diffuses through the CoSi product phase and reacts with

Table 8.2 The integrated diffusion coefficients $\left(\tilde{D}_{\text{int}}\right)$, molar volumes of the Co-silicides (v_m), and the ratio of tracer diffusivities of Si and Co $\left(\frac{\bar{v}_{\text{Co}} D_{\text{Si}}}{\bar{v}_{\text{Si}} D_{\text{Co}}}\right)$ at 1,100 °C in different phases are listed

	Phases	
	Co_2Si	CoSi
$\tilde{D}_{\text{int}}(\text{m}^2/\text{s})$	$(1.5 \pm 0.5) \times 10^{-14}$	$(4.6 \pm 0.3) \times 10^{-14}$
$\frac{D^*_{\text{Si}}}{D^*_{\text{Co}}} = \left(\frac{\bar{v}_{\text{Co}} D_{\text{Si}}}{\bar{v}_{\text{Si}} D_{\text{Co}}}\right)$	0.06 ± 0.025	35 ± 15
v_m (m^3 mol^{-1})	6.56×10^{-6}	6.60×10^{-6}

These are the average values obtained from many different diffusion couples. Therefore, the data considered for Co_2Si in this table are different from the data obtained in a particular diffusion couple, as discussed in the previous example

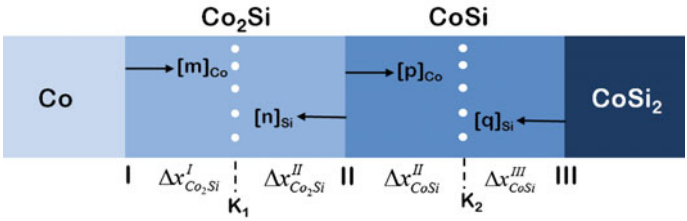

Fig. 8.18 A schematic diagram explaining the physicochemical approach in a Co/$CoSi_2$ diffusion couple

the $CoSi_2$ phase to produce CoSi. Si that reacts with the Co_2Si phase at the interface II is actually produced by the dissociation from the $CoSi_2$ phase at the interface III to produce the CoSi product phase. Therefore, it must be clear that the Co_2Si and CoSi phases at the interfaces grow by consuming the neighboring phase(s) and at the same time become consumed because of the growth of the neighboring phase(s).

In terms of reaction equations, these can be written as:

At the interface I (Co/Co_2Si on the Co_2Si side)

$$2n\text{Co} + n\,[\text{Si}]_d \rightarrow 3n\text{Co}_{2/3}\text{Si}_{1/3}$$

At the interface II (Co_2Si/CoSi on the Co_2Si side)

$$4n\text{Co}_{1/2}\text{Si}_{1/2} \rightarrow n[\text{Si}]_d + 3n\text{Co}_{2/3}\text{Si}_{1/3}$$
$$2m\text{Co}_{1/2}\text{Si}_{1/2} + m\,[\text{Co}]_d \rightarrow 3m\text{Co}_{2/3}\text{Si}_{1/3}$$

At the interface II (Co_2Si/CoSi on the CoSi side)

$$3p\mathrm{Co}_{2/3}\mathrm{Si}_{1/3} \rightarrow p[\mathrm{Co}]_d + 2p\mathrm{Co}_{1/2}\mathrm{Si}_{1/2}$$
$$3q\mathrm{Co}_{2/3}\mathrm{Si}_{1/3} + q[\mathrm{Si}]_d \rightarrow 4q\mathrm{Co}_{1/2}\mathrm{Si}_{1/2}$$

At the interface III (CoSi/$CoSi_2$ on the CoSi side)

$$3p\mathrm{Co}_{1/3}\mathrm{Si}_{2/3} + p[\mathrm{Co}]_d \rightarrow 4p\mathrm{Co}_{1/2}\mathrm{Si}_{1/2}$$
$$3q\mathrm{Co}_{1/3}\mathrm{Si}_{2/3} \rightarrow q[\mathrm{Si}]_d + 2q\mathrm{Co}_{1/2}\mathrm{Si}_{1/2}$$

Therefore, $3n$ moles of the Co_2Si phase are produced at the interface I. At the interface II, $(3m + 3n)$ moles of Co_2Si are produced and at the same time $(3p + 3q)$ moles get consumed. At the same interface, on the other side, $(2p + 4q)$ moles of CoSi are produced; however, $(4n + 2\ m)$ moles get consumed. At the interface III, $(4p + 2q)$ moles of CoSi are produced.

$$\begin{aligned}
&v_m^{\mathrm{Co}_{2/3}\mathrm{Si}_{1/3}} \times 3n = \Delta x^{\mathrm{I}}_{\mathrm{Co_2Si}} \\
&v_m^{\mathrm{Co}_{2/3}\mathrm{Si}_{1/3}} \times (3m + 3n - 3p - 3q) = \Delta x^{\mathrm{II}}_{\mathrm{Co_2Si}} \\
&v_m^{\mathrm{Co}_{\frac{1}{2}}\mathrm{Si}_{\frac{1}{2}}} \times (2p + 4q - 4n - 2m) \\
&v_m^{\mathrm{Co}_{\frac{1}{2}}\mathrm{Si}_{\frac{1}{2}}} \times (4p + 2q)
\end{aligned} \tag{8.23a}$$

The integrated diffusion coefficients can be written as

$$\begin{aligned}
\tilde{D}^{Co_2Si}_{\mathrm{int}} &= \frac{v_m^{Co_2Si}}{2t}\left[N_{Si}^{Co_2Si}m + N_{Co}^{Co_2Si}n\right]\left(\Delta x^{I}_{Co_2Si} + \Delta x^{II}_{Co_2Si}\right) \\
\tilde{D}^{CoSi}_{\mathrm{int}} &= \frac{v_m^{CoSi}}{2t}\left[N_{Si}^{CoSi}p + N_{Co}^{Co_2Si}q\right]\left(\Delta x^{II}_{CoSi} + \Delta x^{III}_{CoSi}\right)
\end{aligned} \tag{8.23b}$$

The ratio of the diffusivities can be written as

$$\begin{aligned}
\left.\frac{D^*_{Si}}{D^*_{Co}}\right|_{Co_2Si} &= \left.\frac{\bar{v}_{Co}D_{Si}}{\bar{v}_{Si}D_{Co}}\right|_{Co_2Si} = \frac{n}{m} \\
\left.\frac{D^*_{Si}}{D^*_{Co}}\right|_{CoSi} &= \left.\frac{\bar{v}_{Co}D_{Si}}{\bar{v}_{Si}D_{Co}}\right|_{CoSi} = \frac{q}{p}
\end{aligned} \tag{8.23c}$$

Using the molar volume values, the integrated diffusion coefficients and the ratio of the intrinsic (or tracer diffusion coefficients), as listed in Table 8.2, we find the values for 100 hrs as

$\Delta x^{\mathrm{I}}_{\mathrm{Co_2Si}} = 32\,\mu\mathrm{m}$, $\Delta x^{\mathrm{II}}_{\mathrm{Co_2Si}} = 133\,\mu\mathrm{m}$, $\Delta x^{\mathrm{II}}_{\mathrm{CoSi}} = 168.5\,\mu\mathrm{m}$, $\Delta x^{\mathrm{II}}_{CoSi} = 294.5\,\mu\mathrm{m}$, $m = 26.8, n = 1.6, p = 0.6$ and $q = 21.0\ \mathrm{mol/m^2}$.

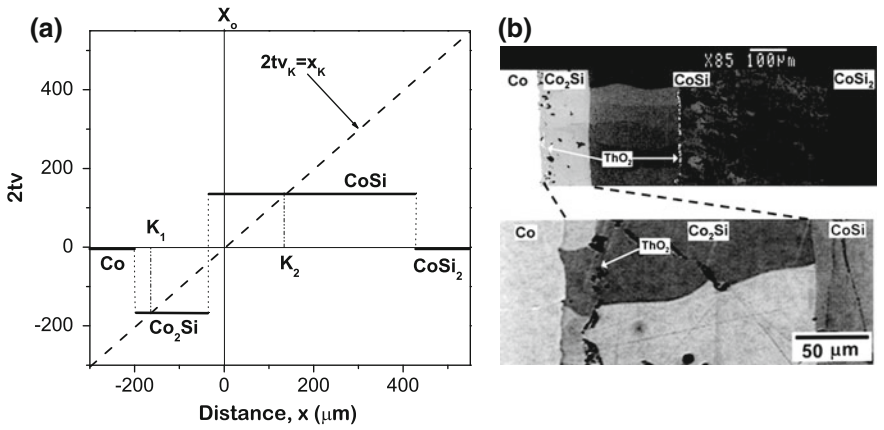

Fig. 8.19 **a** A velocity diagram and **b** the interdiffusion zone showing the location of the marker planes in a Co/$CoSi_2$ diffusion couple [14] annealed at 1100 °C for 100 h

One interesting fact should be noted here that the thicknesses of all the sublayers $\Delta x^{\mathrm{II}}_{\mathrm{Co_2Si}}$ and $\Delta x^{\mathrm{II}}_{\mathrm{CoSi}}$ are positive, despite getting consumed by the neighboring phases at the interface II. This means that both phases will have the Kirkendall marker plane. In other sense, bifurcation of the Kirkendall marker plane is expected. This can be shown with respect to the velocity diagram construction. The velocity of the phases can be estimated as

$$v_m^{\mathrm{Co_2Si}}(n-m) = 2tv_{\mathrm{K}}^{\mathrm{Co_2Si}} = x_{\mathrm{K}}^{\mathrm{Co_2Si}} = -165.3\,\mu\mathrm{m}$$
$$v_m^{\mathrm{CoSi}}(q-p) = 2tv_{\mathrm{K}}^{\mathrm{CoSi}} = x_{\mathrm{K}}^{\mathrm{CoSi}} = 134.6\,\mu\mathrm{m}$$

Note that we have assumed the partial molar volume of the component to be equal to the molar volume of the phase.

It should be noted here that for the velocity diagram plot, we have not determined the initial contact plane—which is not possible to determine correctly—as already explained in Chap. 6. It can be seen that the range of the y and x axes is kept the same such that the straight line $2tv_{\mathrm{K}} = x_{\mathrm{K}}$ will have an angle of 45°. Accordingly, the straight line can just be drawn from one corner to the other as is done in Fig. 8.19a. The location of the initial contact plane is the position at which it intersects $2tv = 0$. The positions of the intersection points by the straight line $2tv_{\mathrm{K}} = x_{\mathrm{K}}$ on the line representing the velocity of the phases indicate the location of the Kirkendall marker plane. Since we have considered the phases with an average composition, the velocity of the phase is drawn by the straight lines. The interdiffusion zone in the Co/$CoSi_2$ phase is shown in Fig. 8.19b. It can be seen that the thicknesses of the phase layers are similar within the range of experimental error. As estimated, both phases contain the Kirkendall marker plane. The presence of duplex morphology is also evident in both phases suggesting the location of the marker planes. Note here that there was a very small dissolution of Si in the

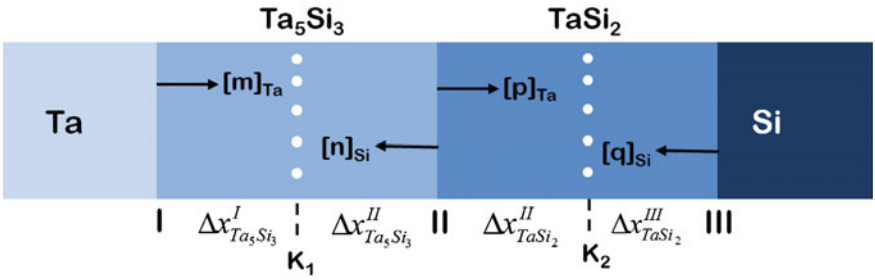

Fig. 8.20 A schematic diagram explaining the physicochemical approach in a Ta/Si diffusion couple

Table 8.3 The integrated diffusion coefficients, $\left(\tilde{D}_{\text{int}}\right)$ molar volumes of the Ta-silicides (v_m) and the intrinsic flux ratios of Si and Ta $\left(\frac{\tilde{v}_{\text{Ta}} D_{\text{Si}}}{\tilde{v}_{\text{Si}} D_{\text{Ta}}}\right)$ at 1,250 °C in different phases are listed [24]

	Phase	
	Ta_5Si_3	$TaSi_2$
$\tilde{D}_{\text{int}}(\text{m}^2/\text{s})$	1.41×10^{-16}	5.02×10^{-14}
$\frac{D^*_{\text{Si}}}{D^*_{\text{Ta}}} = \frac{\tilde{v}_{\text{Ta}} D_{\text{Si}}}{\tilde{v}_{\text{Si}} D_{\text{Ta}}}$	5.8	1.1
v_m (m^3 mol^{-1})	9.48×10^{-6}	8.71×10^{-6}

Co end member, which is neglected in this analysis [16]. This results a minor error in the estimated values.

Now, let us turn to consider a Ta–Si system where there are four intermediate phases [25]; however, only two phases ($TaSi_2$ and Ta_5Si_3) could be detected in the interdiffusion zone. There was an indication that the other phases have a much lower growth rate such that they may be present as very thin layers—but are almost impossible to detect under a scanning electron microscope. Therefore, for our analysis, we can consider the presence of two phases only in the interdiffusion zone, as shown in Fig. 8.20. We shall consider a diffusion couple annealed at 1,250 °C for 9 h. This couple is presented schematically in Fig. 8.20 to explain the dissociation and reaction processes occurring at different interfaces. All details of the integrated diffusion coefficients, the ratio of the diffusivities, and the molar volumes are listed below in Table 8.3.

In the same line of discussion, as described in the previous example, we can write the reaction dissociation equations at the interfaces as

At the interface I

$$\frac{5}{3}\, n\,\text{Ta} + [n]_{\text{Si}} \rightarrow \frac{8}{3}\, n\,\text{Ta}_{5/8}\text{Si}_{3/8}$$

At the interface II (Ta_5Si_3 side)

$$\frac{9}{7}\,m\,\mathrm{Ta}_{1/3}\mathrm{Si}_{2/3} + [m]_{\mathrm{Ta}} \rightarrow \frac{16}{7}\,m\,\mathrm{Ta}_{5/8}\mathrm{Si}_{3/8}$$
$$\frac{15}{7}\,n\,\mathrm{Ta}_{1/3}\mathrm{Si}_{2/3} \rightarrow [n]_{\mathrm{Si}} + \frac{8}{7}\,n\,\mathrm{Ta}_{5/8}\mathrm{Si}_{3/8}$$

Interface II ($TaSi_2$ side)

$$\frac{8}{7}\,q\,\mathrm{Ta}_{5/8}\mathrm{Si}_{3/8} + [q]_{\mathrm{Si}} \rightarrow \frac{15}{7}\,q\,\mathrm{Ta}_{1/3}\mathrm{Si}_{2/3}$$
$$\frac{16}{7}\,p\,\mathrm{Ta}_{5/8}\mathrm{Si}_{3/8} \rightarrow [p]_{\mathrm{Ta}} + \frac{9}{7}\,p\,\mathrm{Ta}_{1/3}\mathrm{Si}_{2/3}$$

Interface III

$$2\,p\,Si + [\,p\,]_{Ta} \rightarrow 3\,p\,Ta_{1/3}Si_{2/3}$$

Accordingly, the thicknesses of the sublayers can be related to the mole of the product phases formed at the different interfaces can be written as

$$\begin{aligned}
&\frac{8}{3}n \times v_m^{\mathrm{Ta_5Si_3}} = \Delta x^{\mathrm{I}}_{\mathrm{Ta_5Si_3}} \\
&\left[\left(\frac{16}{7}m + \frac{8}{7}n\right) - \left(\frac{16}{7}p + \frac{8}{7}q\right)\right] \times v_m^{\mathrm{Ta_5Si_3}} = \Delta x^{\mathrm{II}}_{\mathrm{Ta_5Si_3}} \\
&\left[\left(\frac{15}{7}q + \frac{9}{7}p\right) - \left(\frac{15}{7}n + \frac{9}{7}m\right)\right] \times v_m^{\mathrm{TaSi_2}} = \Delta x^{\mathrm{II}}_{\mathrm{TaSi_2}} \\
&3p \times v_m^{\mathrm{TaSi_2}} = \Delta x^{\mathrm{III}}_{\mathrm{TaSi_2}}
\end{aligned} \tag{8.24a}$$

Following, the integrated diffusion coefficients and the ratio of the diffusivities of the components can be written as

$$\begin{aligned}
\tilde{D}^{Ta_5Si_3}_{\mathrm{int}} &= \frac{v_m^{Ta_5Si_3}}{2t}\left[N_{Ta}^{Ta_5Si_3}\,n + N_{Si}^{Ta_5Si_3}\,m\right]\left(\Delta x^{I}_{Ta_5Si_3} + \Delta x^{II}_{Ta_5Si_3}\right) \\
\tilde{D}^{TaSi_2}_{int} &= \frac{v_m^{TaSi_2}}{2t}\left[N_{Ta}^{TaSi_2}\,q + N_{Si}^{TaSi_2}\,p\right]\left(\Delta x^{II}_{TaSi_2} + \Delta x^{III}_{TaSi_2}\right)
\end{aligned} \tag{8.24b}$$

$$\begin{aligned}
\left.\frac{D^*_{Si}}{D^*_{Ta}}\right|_{Ta_5Si_3} &= \frac{n}{m} \\
\left.\frac{D^*_{Si}}{D^*_{Ta}}\right|_{TaSi_2} &= \frac{q}{p}
\end{aligned} \tag{8.24c}$$

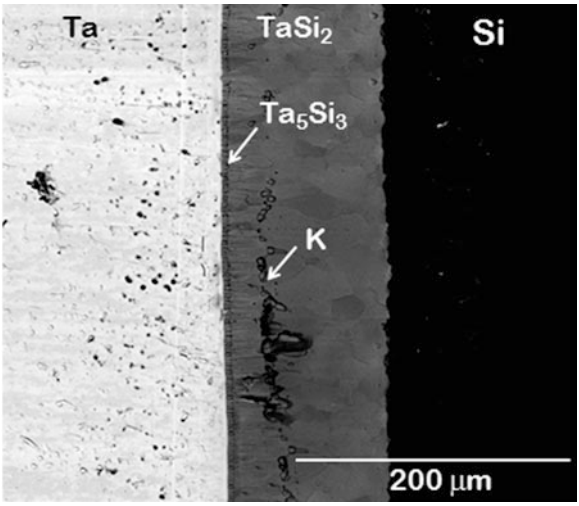

Fig. 8.21 Interdiffusion zone of the Ta/Si diffusion couple annealed at 1,250 °C for 9 h

Using the values in the Table 8.3 for 9 h, we get

$$\Delta x^{\mathrm{I}}_{\mathrm{Ta_5Si_3}} = 64.07,\ \Delta x^{\mathrm{II}}_{\mathrm{Ta_5Si_3}} = -63.52,\ \Delta x^{\mathrm{II}}_{\mathrm{TaSi_2}} = 42.7 \text{ and } \Delta x^{\mathrm{III}}_{\mathrm{TaSi_2}} = 78.15\ \mu\mathrm{m}$$
$$m = 0.437, n = 2.535, p = 2.99 \text{ and } q = 3.29\ \mathrm{mol/m^2}.$$

Unlike the example, as discussed before, all sublayer thicknesses do not have positive values. This would indicate that $\Delta x^{\mathrm{II}}_{\mathrm{Ta_5Si_3}}$ gets consumed at the interface II because of the growth of $\Delta x^{\mathrm{II}}_{\mathrm{TaSi_2}}$. Therefore, the total thickness of the Ta_5Si_3 phase is $\Delta x^{\mathrm{I}}_{\mathrm{Ta_5Si_3}} + \Delta x^{\mathrm{II}}_{\mathrm{Ta_5Si_3}} = 0.55$ μm. This further means that there will be a Kirkendall marker plane in the $TaSi_2$ phase and no marker plane in the Ta_5Si_3 phase. This is indeed to be found also in the Ta/Si couple as shown in Fig. 8.21. The location of the marker plane is evident from the presence of pores and the duplex morphology, as discussed in greater depth in Chap. 6.

Now, let us consider the Ag–Zn system, as shown in Figs. 8.10a and 8.12. The Zn/Ag couple was annealed at 370 °C for 5 h, and analysis can be done to understand the reason for not finding any Kirkendall marker plane in the β-AgZn phase [13, 26]. The composition profile is given in Fig. 8.22. It can be seen that the phases have a wide homogeneity range. To simplify the analysis, we consider an average composition of the phases, which is estimated from

$$N^{\theta}_{\mathrm{Ag}}\Big|_{\mathrm{ave}} = \frac{\int_{N^{-\theta}_{\mathrm{Ag}}}^{N^{+\theta}_{\mathrm{Ag}}} N_{\mathrm{Ag}}\,dx}{\Delta x_{\theta}} \tag{8.25}$$

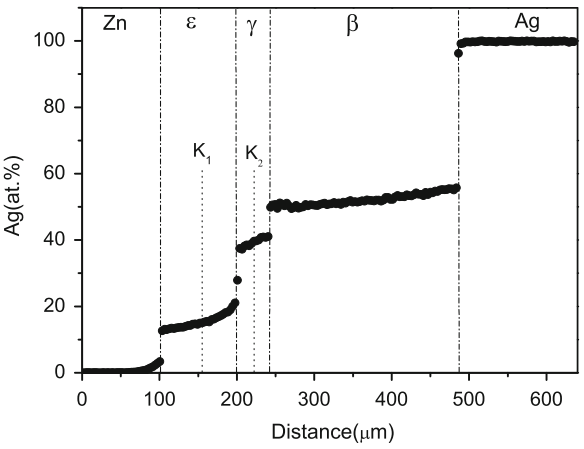

Fig. 8.22 Composition profile of the Ag/Zn diffusion couple annealed at 370 °C for 5 h

where θ is the phase of interest, $N_{Ag}^{-\theta}$ and $N_{Ag}^{+\theta}$ are the phase boundary compositions, and Δx_θ is the thickness of the interested phase. The estimated average compositions of the ε, γ and β phases are $Ag_{0.154}Zn_{0.846}$, $Ag_{0.394}Zn_{0.606}$, and $Ag_{0.521}Zn_{0.479}$, respectively. For our analysis without complication, we ignore the dissolution of Ag in Zn and Zn in Ag, since the composition profiles developed in these solid solutions are small.

The schematic diffusion couple is presented above in Fig. 8.23. Based on the average compositions of the phases, the reaction/dissociation equations at different interfaces can be written as

Interface I—$Zn/AgZn_3$ ($AgZn_3$ side)

$$5.49nZn + [n]_{Ag} \rightarrow 6.49nAg_{0.154}Zn_{0.846}(\varepsilon)$$

Reaction of Ag with Zn

Interface II—$AgZn_3/Ag_5Zn_8$ ($AgZn_3$ side)

$$0.64mAg_{0.394}Zn_{0.606}\ (\gamma) + [m]_{Zn} \rightarrow 1.64mAg_{0.154}Zn_{0.846}(\varepsilon)$$

Reaction of Zn with Ag_5Zn_8

$$3.53nAg_{0.394}Zn_{0.606}(\gamma) \rightarrow [n]_{Ag} + 2.53nAg_{0.154}Zn_{0.846}(\varepsilon)$$

Dissociation of Ag from Ag_5Zn_8

Interface II—$AgZn_3/Ag_5Zn_8$ (Ag_5Zn_8 side)

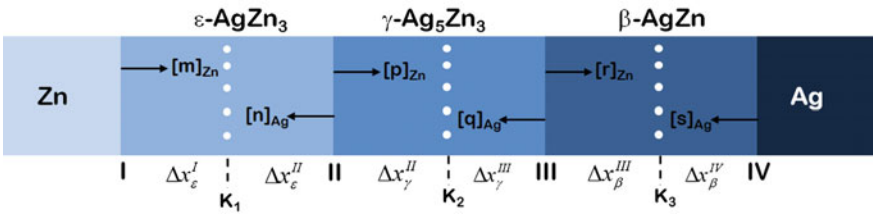

Fig. 8.23 A schematic diagram explaining the physicochemical approach in the Ag/Zn diffusion couple

$$1.64p\mathrm{Ag}_{0.154}\mathrm{Zn}_{0.846}(\varepsilon) \rightarrow [p]_{\mathrm{Zn}} + 0.64p\mathrm{Ag}_{0.394}\mathrm{Zn}_{0.606}(\gamma)$$

Dissociation of Zn from $AgZn_3$

$$2.53q\mathrm{Ag}_{0.154}\mathrm{Zn}_{0.846}(\varepsilon) + [q]_{\mathrm{Ag}} \rightarrow 3.53q\mathrm{Ag}_{0.394}\mathrm{Zn}_{0.606}(\gamma)$$

Reaction of Ag with $AgZn_3$

Interface III—Ag_5Zn_8/AgZn (Ag_5Zn_8 side)

$$3.10p\mathrm{Ag}_{0.521}\mathrm{Zn}_{0.479}(\beta) + [p]_{\mathrm{Zn}} \rightarrow 4.10p\mathrm{Ag}_{0.394}\mathrm{Zn}_{0.606}(\gamma)$$

Reaction of Zn with AgZn

$$4.77q\mathrm{Ag}_{0.521}\mathrm{Zn}_{0.479}(\beta) \rightarrow [q]_{\mathrm{Ag}} + 3.77q\mathrm{Ag}_{0.394}\mathrm{Zn}_{0.606}(\gamma)$$

Dissociation of Ag from AgZn

Interface III—Ag_5Zn_8/AgZn (AgZn side)

$$4.10r\mathrm{Ag}_{0.394}\mathrm{Zn}_{0.606}(\gamma) \rightarrow [r]_{\mathrm{Zn}} + 3.10r\mathrm{Ag}_{0.521}\mathrm{Zn}_{0.479}(\beta)$$

Dissociation of Zn from Ag_5Zn_8

$$3.77s\mathrm{Ag}_{0.394}\mathrm{Zn}_{0.606}\ (\gamma) + \ [s]_{\mathrm{Ag}} \rightarrow 4.77s\mathrm{Ag}_{0.521}\mathrm{Zn}_{0.479}(\beta)$$

Reaction of Ag with Ag_5Zn_8

Interface IV—AgZn/Ag (AgZn side)

$$1.09r\mathrm{Ag} + [r]_{\mathrm{Zn}} \rightarrow 2.09r\mathrm{Ag}_{0.521}\mathrm{Zn}_{0.479}(\beta)$$

Reaction of Zn with Ag.

Here, m, n, p, q, r, and s are the fluxes (moles/m^2) of the components as shown in Fig. 8.23. The product phases produced at different interfaces can be related to the thicknesses of the sublayers as

$$\begin{aligned}
v_m^{\varepsilon}(6.49n) &= \Delta x_{\varepsilon}^{\mathrm{I}} \\
v_m^{\varepsilon}(1.64m + 2.53n - 1.64p - 2.53q) &= \Delta x_{\varepsilon}^{\mathrm{II}} \\
v_m^{\gamma}(0.64p + 3.53q - 0.64m - 3.53n) &= \Delta x_{\gamma}^{\mathrm{II}} \\
v_m^{\gamma}(4.10p + 3.77q - 4.10r - 3.77s) &= \Delta x_{\gamma}^{\mathrm{III}} \\
v_m^{\beta}(3.10r + 4.77s - 3.10p - 4.77q) &= \Delta x_{\beta}^{\mathrm{III}} \\
v_m^{\beta}(2.09r) &= \Delta x_{\beta}^{\mathrm{IV}}
\end{aligned}$$

The molar volumes of the ε, γ and β phases are 9.20×10^{-6}, 9.44×10^{-6} and 9.46×10^{-6} m^3/mol. The sublayer thicknesses in the ε and γ phases measured directly from the Ag–Zn diffusion couple as shown in Fig. 8.24 are $\Delta x_{\varepsilon}^{\mathrm{I}} = 48.6$, $\Delta x_{\varepsilon}^{\mathrm{II}} = 50.2$, $\Delta x_{\gamma}^{\mathrm{II}} = 16.65$, $\Delta x_{\gamma}^{\mathrm{III}} = 24.45$ and $\left(\Delta x_{\beta}^{\mathrm{III}} + \Delta x_{\beta}^{\mathrm{IV}}\right) = 244\,\mu\mathrm{m}$. The ratio of the diffusivities in the β-AgZn phase was estimated using an incremental couple as $\frac{r}{s} = \frac{V_{\mathrm{Ag}} D_{\mathrm{Zn}}}{V_{\mathrm{Zn}} D_{\mathrm{Ag}}} = 6.5$. From these, the rest of the parameters are estimated as $m = 19.62$, $n = 0.81$, $p = 13.88$, $q = 2.37$, $r = 13.52$, $s = 2.08$ mol/m^2, and $\Delta x_{\beta}^{\mathrm{III}} = -23.72$ and $\Delta x_{\beta}^{\mathrm{IV}} = 267.72$ mm. Therefore, the negative value of $\Delta x_{\beta}^{\mathrm{III}}$ is suggestive of the consumption of the sublayer by the neighboring phase and the absence of the Kirkendall marker plane in the β phase.

Now, let us consider different locations of the marker planes and the kind of morphology to be expected in the interdiffusion zone. Our discussion shall be based upon only two product phases in the interdiffusion zone; the description is, however, the same when a different number of phases are formed. Typically, we expect to find one of the three examples given in Fig. 8.24.

Suppose, two phases (A_2B and AB_2) are grown in the interdiffusion zone of a hypothetical A/B diffusion couple. There is a possibility that the marker planes are present in both the phases, as shown in Fig. 8.24a, meaning that the thicknesses of all the sublayers are positive and duplex morphology should be expected in both the phases. It should be noted here that finding more than one Kirkendall plane in an interdiffusion zone is not very common—with very few rare examples being found till date [27]. In most cases, a single marker plane is present in one of the phases—as shown in Fig. 8.24b—which signifies that the thicknesses of the sublayers $\Delta x_{\mathrm{A_2B}}^{\mathrm{I}}$ and $\Delta x_{\mathrm{A_2B}}^{\mathrm{II}}$ are positive in the A_2B phase. $\Delta x_{\mathrm{AB_2}}^{\mathrm{II}}$ is negative, which

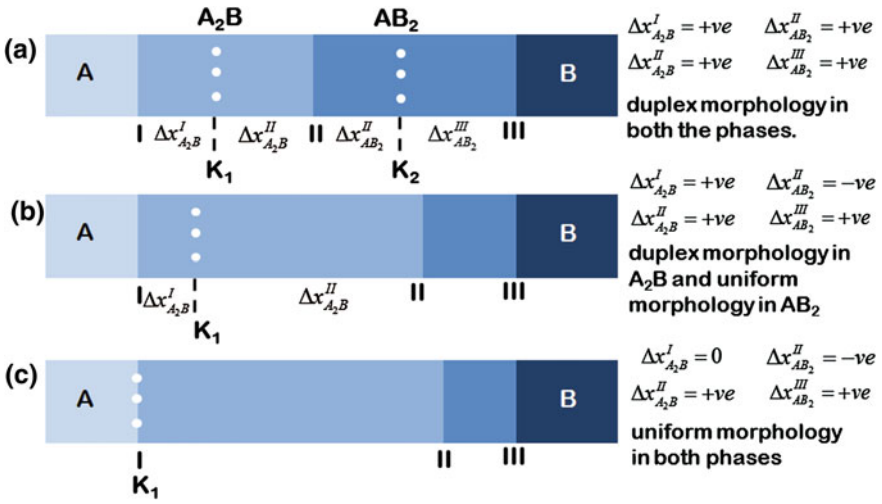

Fig. 8.24 Schematic representation of the diffusion couple explaining the situation for finding **a** bifurcation of the marker plane **b** a single Kirkendall marker plane in the A_2B phase and **c** a single marker plane at A/A_2B phase

means that this part is consumed because of the growth of the $\Delta x^{\mathrm{II}}_{\mathrm{A_2B}}$. However, $\Delta x^{\mathrm{III}}_{\mathrm{AB_2}}$ is positive. This suggests that duplex morphology is to be expected in the A_2B phase and a uniform morphology is expected in the AB_2 phase. There could be many examples where the marker plane is present at one of the interfaces of the end-member/product phase, as shown in Fig. 8.24c. Very frequently, it is concluded (based on the similar location of the marker plane) that one of the components has a much higher diffusion rate compared to the other in both phases. This is not correct. For example, if the marker plane is present at the A/A_2B interface, it is true that A has a much higher diffusion rate compared to B in the A_2B phase. However, it is not indicative of the relative mobilities of the components in the AB_2 phase. There could be a comparable diffusion rate of both the components in this phase. Due to the significantly higher diffusion rate of A and negligible diffusion rate of B in the A_2B phase, $\Delta x^{\mathrm{I}}_{\mathrm{AB_2}}$ will be negligible and $\Delta x^{\mathrm{II}}_{\mathrm{AB_2}}$ will be almost equal to the total thickness of the A_2B phase. Moreover, due to the very high flux of A through this phase, the growth rate of this product phase is very high at the interface II and might consume the whole of $\Delta x^{\mathrm{II}}_{\mathrm{AB_2}}$ and a part of $\Delta x^{\mathrm{III}}_{\mathrm{AB_2}}$ such that $\Delta x^{\mathrm{II}}_{\mathrm{AB_2}}$ will have a negative value. Therefore, both the phases will have a uniform morphology. It should be noted here that, sometimes, even if the possibility of bifurcation of the marker plane is expected in an interdiffusion zone, the markers in both the phases might not be found. This was seen in the Cu–Sn system, where the Cu_3Sn and Cu_6Sn_5 phases are seen to be growing at the interdiffusion zone [28]. The marker plane was found only in the Cu_6Sn_5 phase; however, according to the analysis based on the diffusion parameters in the phases, the

marker plane should be present in both the phases. To find the marker planes in both the phases, it is important that both phases should start growing together from the beginning to trap the markers. This is, in general, found in bulk diffusion couples, as discussed till now. In thin films, on the other hand, sequential phase growth is very frequently reported. The presence of the marker plane only in the Cu_6Sn_5 phase, however, indicates the sequential growth of the phases, where the Cu_3Sn phase, most probably, started growing after some incubation period. If this is true, once all the markers get trapped in the Kirkendall marker plane in the Cu_6Sn_5 phase, no markers will be left in the Cu_3Sn phase after it starts growing.

8.5 Effect of Electrical Current on the Microstructural Evolution of the Diffusion Zone

The physicochemical approach can also be utilized to rationalize the effect of additional driving forces, such as electric field, on the growth of interfacial phases. Figure 8.25 shows a cross section of the component with the directions of the current and electron flux. The electron flux enters the component from the source contact and leaves from the drain contact. In the forthcoming analysis of the effect of the electron flow on the IMC, growth only the on the printed wiring board (PWB) side is considered. This is because, at the component side, the presence of Ag finish will make the analysis less quantitative.

Figure 8.26 shows the interfacial microstructures from solder—PWB interfaces from the samples that have been annealed at 110 °C for 750 h and both the drain as well as source contacts after 750 h of constant current stressing.

Due to the relatively complex geometry of the interconnections and the differences in cross-sectional areas, the current crowding effects and thus the differences in current densities cannot be easily addressed. However, even if only the direction of the electron flux is taken into consideration, the marked differences in the total IMC growth kinetics as well as the relative thicknesses of the Cu_6Sn_5 and Cu_3Sn intermetallic compounds can be observed when these differences are compared with the results obtained using the diffusion couple experiments [29, 30]. Closer examination of Table 8.4 and Fig. 8.26 reveals that when the flow of electrons is toward the PWB, the η and ε phase layers are almost of the same thickness, whereas in the opposite situation, the thickness of Cu_3Sn is drastically reduced.

The thickness ratio of Cu_6Sn_5 to Cu_3Sn is unusually high in the case of the annealed samples (Table 8.4) when compared to the earlier results from the Cu/Sn(X) diffusion couples [31–35]. It is known that impurity and alloying components can drastically change the growth kinetics of the IMC compounds [32]. Hence, it is not surprising that the IMC ratio differs from that observed with high purity materials. Based on our previous experiments, it is known that alloying components (like Ni) in copper increase the Sn flux through Cu_6Sn_5 but have no measurable effect on the intrinsic fluxes inside Cu_3Sn. This, in turn, results in a

Fig. 8.25 SEM micrograph of the structure of the component used in the electromigration study

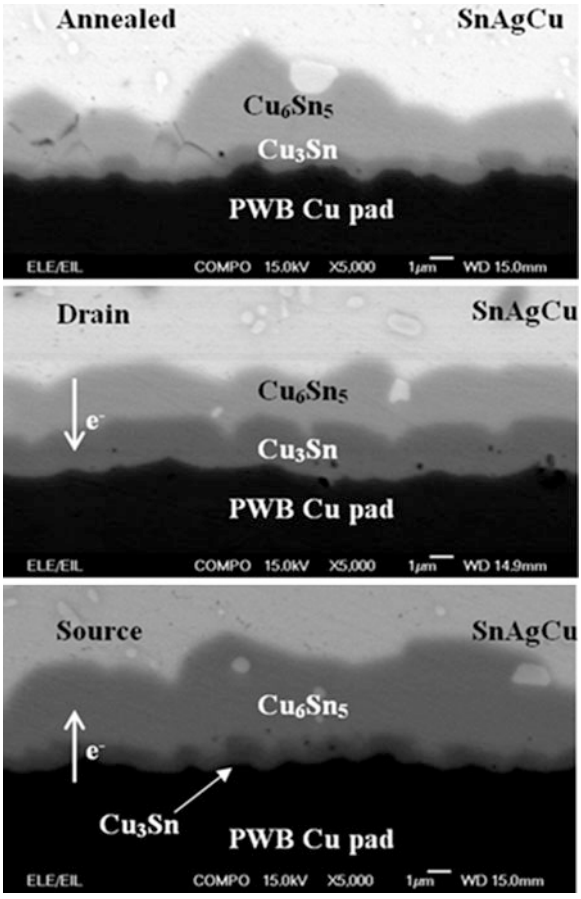

Fig. 8.26 SEM micrograph showing the interfacial reaction layer structure depending on the direction of the electron flux [29]

lower growth rate of Cu_3Sn than in the case of a pure Cu/Sn diffusion couple. The decrease in the growth rate of Cu_3Sn can be understood when it is noticed that the growth of the reaction layers in multiphase diffusion couples is dependent on each other. Thus, when the formation rate of Cu_6Sn_5 at the Cu_3Sn/Cu_6Sn_5 interface increases, more and more Cu_3Sn is consumed by the growing η layer. As the fluxes of either Sn or Cu inside Cu_3Sn are not significantly altered, this results in the observed growth behavior. A similar (but slightly different) effect using the electron flux can be observed here as discussed below. Regarding the annealed

Table 8.4 Thickness data of the intermetallic compounds grown at the interface

	Cu_3Sn	Cu_6Sn_5	Cu_6Sn_5 to Cu_3Sn ratio
No current	0.8 μm 0.093 mol/m^2	3 μm 0.283 mol/m^2	3.8
Constant current from PWB	2.1 μm 0.244 mol/m^2	2.3 μm 0.217 mol/m^2	1.1
Constant current from solder	0.9 μm (∼no change) 0.1 mol	3.8 μm 0.36 mol/m^2	4.2

samples, it is to be noted that in this case, the Cu–Sn IMCs are growing between the Cu and SnAgCu solder instead of between Cu and pure Sn. Based on the experimental results [34], it is known that the thickness of Cu_3Sn is smaller when growth takes place in the Cu/SnAgCu diffusion couple than in the Sn/Cu diffusion couple at the same temperature. This can be understood when considering how the presence of Ag and Cu in solder affects the activities of the diffusing components. The presence of Cu in the solder decreases the driving force for diffusion of Cu from the Cu-substrate to the solder as the activity difference decreases. Likewise, the lowering of the activity of Sn in the solder (because of the presence of Ag) reduces the driving force for diffusion of Sn toward the Cu-substrate, thus reducing the Sn flux. These two effects combine to produce the observed difference between the Cu/Sn and Cu/SnAgCu reaction couples. Finally, it is emphasized that also the slightly lower temperature used here (110 °C instead of 125 °C which is used in the reference cases [34, 35]) will itself contribute to the observed smaller thickness ratio of Cu_3Sn to Cu_6Sn_5.

From the results of the steady current experiments, it can be seen that in the drain contact, the electron flux comes from the solder side to the interface. Thus, the PWB pad is acting as the anode, meaning that the Sn flux toward the PWB is increased in both IMC layers whereas the flux of Cu from the PWB is decreased, which, based on the experimental results, seems to favor the growth of Cu_3Sn. This can be analyzed in more detail with the help of Fig. 8.27 and the following reaction equations.'

The reaction scheme

The reactions occurring at different interfaces of the reaction couple, as shown in Fig. 8.27, can be expressed as follows

Interface I:

$$3q\mathrm{Cu} + q[\mathrm{Sn}]_d \rightarrow 4q\mathrm{Cu}_{3/4}\mathrm{Sn}_{1/4}$$

Interface II Cu_3Sn side:

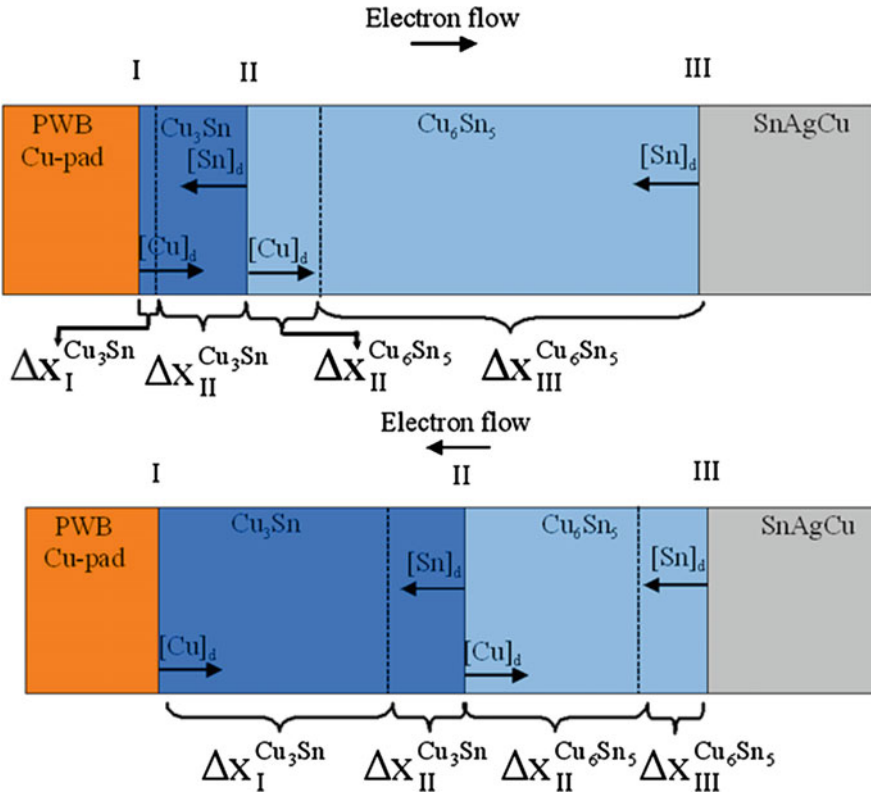

Fig. 8.27 Schematic presentation of the interfacial reactions occurring in the reaction couple

$$\frac{11}{9}p\mathrm{Cu}_{6/11}\mathrm{Sn}_{5/11} + p[\mathrm{Cu}]_d \rightarrow \frac{20}{9}p\mathrm{Cu}_{3/4}\mathrm{Sn}_{1/4}$$
$$\frac{11}{3}q\mathrm{Cu}_{6/11}\mathrm{Sn}_{5/11} \rightarrow q[\mathrm{Sn}]_d + \frac{8}{3}q\mathrm{Cu}_{3/4}\mathrm{Sn}_{1/4}$$

Interface II Cu_6Sn_5 side:

$$\frac{20}{9}r\mathrm{Cu}_{3/4}\mathrm{Sn}_{1/4} \rightarrow r[\mathrm{Cu}]_d + \frac{11}{9}r\mathrm{Cu}_{6/11}\mathrm{Sn}_{5/11}$$
$$\frac{8}{3}s\mathrm{Cu}_{3/4}\mathrm{Sn}_{1/4} + s[\mathrm{Sn}]_d \rightarrow \frac{11}{3}s\mathrm{Cu}_{6/11}\mathrm{Sn}_{5/11}$$

Interface III:

$$\frac{5}{6}r\mathrm{Sn} + r[\mathrm{Cu}]_d \rightarrow \frac{11}{6}r\mathrm{Cu}_{6/11}\mathrm{Sn}_{5/11}$$

Table 8.5 Summary of the experimental results

	Cu_6Sn_5 (μm)	Cu_3Sn (μm)	IMC tot (μm)
After soldering			
No current	1	0.1	1.1
Drain	1	0.1	1.1
Source	1	0.1	1.1
1,500 Cycles			
No current	1.8	1.4	3.2
Drain	2.4	1.2	3.6
Source	3.6	0.3	3.9
3,000 Cycles			
No current	1.9	1.9	3.8
Drain	2.7	1.5	4.2
Source	4.4	0.5	4.9

Here, p and q are the moles of Cu and Sn, respectively, transferred per unit area through the Cu_3Sn phase during the total diffusion time t. Similarly, r and s are the number of moles of Cu and Sn transported during interaction per unit area through the Cu_6Sn_5-phase layer. From the equations written above, it is clear that at the interface II, not only $\left(\frac{20}{9}p+\frac{8}{3}q\right)$ moles of Cu_3Sn grow, but also $\left(\frac{20}{9}r+\frac{8}{3}s\right)$ moles get consumed because of the growth of the Cu_6Sn_5 phase. Similarly, $\left(\frac{11}{9}r+\frac{11}{3}s\right)$ moles of Cu_6Sn_5 grow at the same interface, but $\left(\frac{11}{9}p+\frac{11}{3}q\right)$ moles get consumed by the Cu_3Sn phase.

The thickness of the parts of the product phase layers resulting from the interfacial reactions given above can be expressed as

$$
\begin{aligned}
&4q \times v_m^{Cu_3Sn} = \Delta x_{\mathrm{I}}^{Cu_3Sn}\\
&\left(\frac{20}{9}p+\frac{8}{3}q-\frac{20}{9}r-\frac{8}{3}s\right) \times v_m^{Cu_3Sn} = \Delta x_{\mathrm{II}}^{Cu_3Sn}\\
&\left(\frac{11}{9}r+\frac{11}{3}s-\frac{11}{9}p-\frac{11}{3}q\right) \times v_m^{Cu_6Sn_5} = \Delta x_{\mathrm{II}}^{Cu_6Sn_5}\\
&\frac{11}{6}r \times v_m^{Cu_6Sn_5} = \Delta x_{\mathrm{III}}^{Cu_6Sn_5}
\end{aligned}
$$

where $\Delta x_{\mathrm{I}}^{Cu_3Sn}$ and $\Delta x_{\mathrm{II}}^{Cu_3Sn}$ are the thicknesses of the sublayers in the Cu_3Sn phase. $\Delta x_{\mathrm{II}}^{Cu_6Sn_5}$ and $\Delta x_{\mathrm{III}}^{Cu_6Sn_5}$ are the thicknesses of sublayers in the Cu_6Sn_5 phase. These sublayers are separated by the Kirkendall marker planes in these phases. In Table 8.5, the experimental results about the effect of the electron flow on the growth of the IMCs are presented in a different way. In addition to thickness, the amount of each phase has been tabulated in terms of mole/m^2 for the sake of discussion.

PWB as the anode

Let us first consider that there is an equal increase in the flux of Sn and an equal decrease in the flux of Cu in both the phases. First, the two cases will be addressed separately and then the combined effect of the changes in the Cu and Sn fluxes is addressed.

(i) Increase in the Sn flux through the phases:

Owing to the diffusion of Sn, 4 parts (in terms of moles) of the Cu_3Sn product phase will grow at the interface I plus a further 8/3 parts at the interface II by consuming the Cu_6Sn_5 phase. On the other hand, 8/3 parts will get consumed because of the growth of the Cu_6Sn_5 phase at the interface II. So, in total, there will be a net gain of 4 parts of the Cu_3Sn phase in this case.

Similarly, 11/3 parts of the Cu_6Sn_5 phase will grow at the interface II and the same amount will get consumed because of the growth of the Cu_3Sn phase at that interface. So, there should be no net change in the layer thickness of the Cu_6Sn_5 phase.

(ii) Decrease in the Cu flux through the phases:

If the flow of Cu decreases at the same rate through both the phases, there will be 20/9 parts (in terms of moles) less production of Cu_3Sn at the interface II. Further, because of the decreased diffusion rate of Cu through the Cu_6Sn_5 phase, there will be 20/9 less consumption of the Cu_3Sn phase at the interface II. So, there should be no net change in the layer thickness of the Cu_3Sn phase because of the flow of electrons from solder to the PWB.

On the other hand, as a result of the lower production of the Cu_3Sn phase at the interface II, there will be 11/9 parts less consumption of the Cu_6Sn_5 phase at that interface. At the same time (because of the decreased flow rate of Cu through the Cu_6Sn_5 phase), there will 11/9 parts less production of the Cu_6Sn_5 phase due to the dissociation of the Cu_3Sn phase at the interface II. Finally, there will be lower production of 11/6 parts of the Cu_6Sn_5 phase at the interface III. So, there should be a net loss in the thickness of the Cu_6Sn_5 phase compared to the situation when there is no flow of electrons.

(iii) Combined effect of Sn and Cu fluxes

Thus, if the Cu and Sn fluxes are affected similarly in both the phases, then for every 4 parts of Cu_3Sn phase increase there will be a corresponding 11/6 parts decrease in the layer thickness of the Cu_6Sn_5 phase. This means that for a one-part increase in the thickness of the Cu_3Sn phase, there will be a corresponding 0.46 parts decrease in the thickness of the Cu_6Sn_5 phase. In our experimental results, we actually get for a 0.151 parts (mol/m^2) increase in the thickness of the Cu_3Sn phase a corresponding decrease of 0.066 parts in the Cu_6Sn_5 phase. This can be put in another way: for a 1-part Cu_3Sn phase increase, we get 0.44 parts of decrease in the Cu_6Sn_5 phase. This is very close to the analysis presented above and can thus

be taken to indicate that the components (Sn and Cu) are indeed affected in a similar fashion by the electron flow. To conclude, it is now self-evident that it is time to reexamine the assumption that Sn should be strongly affected by the electron flux owing to its higher effective valence (Z*).

PWB as the cathode

Again, we consider there to be an equal decrease of Sn flux and an increase of Cu in both the phases. The good match between the analysis results based on this assumption with the experimental results, shown above, gives us further confidence that this approach is justified.

(i) Increase in Cu flux through the phases:

When the amount of Cu_3Sn increases by 20/9 parts (in moles) by consuming the Cu_6Sn_5 phase at the interface II because of the increase of Cu flux, 20/9 parts of the same phase will get consumed because of the growth of the Cu_6Sn_5 phase at the same interface. So, there will be no net gain or loss in the thickness of the Cu_3Sn phase because of the increase in the diffusion rate of Cu. Owing to the increase in the flow of Cu through the Cu_3Sn phase, the increased consumption of 11/9 of the Cu_6Sn_5 phase will occur at the interface II. However, at the same time, 11/9 parts of the same phase will grow by dissociation of the Cu_3Sn phase, because of the increase in flow of Cu through this phase. A further increase of 11/6 parts of the Cu_6Sn_5 phase will occur due to the increase in the flow of Cu through the η phase. So, there should be no net gain in the thickness of the Cu_3Sn phase, but a net gain of 11/6 parts in the thickness of the Cu_6Sn_5 phase.

(ii) Decrease in Sn flux through the phases:

Owing to the decreased diffusion rate of Sn through the Cu_3Sn phase, there will be a corresponding 4 parts decrease in the layer thickness. Similarly, there will be 8/3 parts less produced at the interface II caused by the dissociation of the Cu_6Sn_5 phase. Furthermore, because of the decreased diffusion rate of Sn through the Cu_6Sn_5 phase, the consumption of the same phase will be 8/3 parts less at the same interface. So, the net loss for the Cu_3Sn should be 4 parts.

Because of the decrease of Sn flux through the Cu_6Sn_5 phase, there will be 11/3 parts less production of the phase at the interface II by consuming the Cu_3Sn phase. At the same time, there will be 11/3 parts less consumption of the same phase because of the low diffusion rate of Sn through the Cu_3Sn phase. So, there should be no net gain in the Cu_6Sn_5 phase layer thickness because of low flux of Sn through both the phases.

(iii) Combined effect of Sn and Cu fluxes

When we consider the increase in the flow of Cu and the corresponding decrease in the flow of Sn to occur equally through both the phases, there will be a net gain of 11/6 parts in the thickness of Cu_6Sn_5 and a net decrease of 4 parts in the thickness of the Cu_3Sn phase. However, the diffusion rate of Sn is known to be

Table 8.6 Summary of the experimental and theoretical results

PWB side acting as	Effect of electron flux				Theoretical result		Experimental result	
	Flux of Sn in ε	Flux of Cu in ε	Flux of Sn in η	Flux of Cu in η	Thickness of ε	Thickness of η	Thickness of ε	Thickness of η
Anode	⇑	⇓	⇑	⇓	⇑	⇓	⇑	⇓
Cathode	⇓	⇑	⇓	⇑	± 0	⇑	±0	⇑

small compared to that of Cu in the Cu_3Sn phase, as shown in the ratios of the tracer diffusion coefficients [28]

$$\left.\frac{D^*_{Cu}}{D^*_{Sn}}\right|_{Cu_3Sn} = \frac{p}{q} \approx 30$$

$$\left.\frac{D^*_{Cu}}{D^*_{Sn}}\right|_{Cu_6Sn_5} = \frac{r}{s} \approx 0.35$$

Consequently, the role of Sn in this phase can be neglected—especially in this particular case as the diffusion of Sn is further hindered by the electron flux.

Overall, therefore, there should be an increase in the layer thickness of the Cu_6Sn_5 phase, which is what we see in the experiment. The results from the above analysis and from the experiments are summarized in Table 8.6.

References

1. E.O. Kirkendall, Diffusion of Zinc in Alpha Brass, Transaction of AIME 147 (1942) pp. 104
2. A.D. Smigelkas and E.O. Kirkendall, Zinc diffusion in alpha brass, Transaction of AIME 171 (1947) 130
3. G.F. Bastin and G.D. Rieck, Metallurgical Transactions 5 (1974) 1817
4. T. Shimozaki, Y. Goda, Y. Wakamatsu and M. Onishi, Defects and Diffusion Forum 95-98 (1993) 629
5. J.-F. Cornet and D. Calais, Journal of Physics and Chemistry of Solids 33 (1972) 1675-84
6. F.J.J. van Loo, B. Pieraggi and R.A. Rapp, Acta Metallurgica et Materialia 38 (1990) 1769
7. M.J.H van Dal, A.M. Gusak, C. Cserháti, A.A. Kodentsov and F.J.J van Loo, Physical Review Letters 86 (2001) 3352
8. M.J.H. van Dal, A.M. Gusak, C. Cserháti, A.A. Kodentsov and F.J.J. van Loo, Philosophical Magazine A, 82 (2002) 943
9. M.J.H. van Dal, M.C.L.P Pleumeekers, A.A. Kodentsov and F.J.J. van Loo, Acta Materialia 48 (2000) 385
10. M.J.H. van Dal, Microstructural stability of the Kirkendall plane, PhD thesis, Technische Universetiet Eindhoven, The Netherlands, 2001.
11. A. Paul, A.A. Kodentsov and F.J.J. van Loo, Acta Materialia 52 (2004) 4041
12. A. A. Kodentsov, A. Paul, Frans J.J. van Loo, Zeitschrift für Metallkunde 95 (2004) 258
13. A. Paul, The Kirkendall effect in solid state diffusion, PhD thesis, Technische Universetiet Eindhoven, The Netherlands, 2004.
14. M.J.H. van Dal, D.G.G.M. Huibers, A.A. Kodentsov, F.J.J. van Loo, Intermetallics 9 (2001) 409

15. M.J.H. van Dal, A.A. Kodentsov and F.J.J. van Loo, Intermetallics 9 (2001) 451
16. A. Paul, M.J.H. van Dal, A.A. Kodentsov and F.J.J. van Loo, Acta Materialia 52 (2004) 623-
17. L. Höglund, & J. Ågren, Acta Materialia 49 (2001) 1311
18. W.J. Boettinger, J.E. Guyer, C.E. Campbell and G.B. McFadden, Proceeding of the Royal Society London A 463 (2007) 3347
19. J.H. Gülpen, A.A. Kodentsov, F.J.J. van Loo, Zeitschrift für Metallkunde 86 (1995) 530.
20. C. Cserháti, A. Paul, A.A. Kodentsov, M.J.H. van Dal, F.J.J. van Loo, Intermetallics 11 (2003) 291-297.
21. C. Ghosh and A. Paul, Acta Materialia 55 (2007) 1927
22. F.J.J. van Loo, Acta Metallurgica 18 (1970) 1107
23. A. Paul, A.A. Kodentsov and F.J.J. van Loo, Intermetallics, 14 (2006) 1428
24. H. Okamoto, Journal of Phase Equilibria and diffusion 25 (2004) 394
25. S. Roy and A. Paul, Philosophical Magazine, 92 (2012) 4215
26. A.A. Kodentsov, A. Paul, and F.J.J. van Loo, Defects and Diffusion Forum 258-260 (2006) 182
27. A. Paul, Journal of Materials Science: Materials in Electronics 22 (2011) 833
28. A. Paul, C. Ghosh and W.J. Boettinger, Metallurgical and Materials Transactions A 42A (2011) 952
29. T. Laurila, J. Karppinen, V.Vuorinen, A. Paul and M. Paulasto-Kröckel, Journal of Electronic Materials 40 (2011) 1517
30. T. Laurila, J. Karppinen, V. Vuorinen, J. Li, A.Paul and M. Paulasto-Kröckel, Journal of Electronic Materials 41 (2012)
31. J. Dekker, A. Lodder and J. van Ek, Physical Review B 56 (1997) 12167-12177
32. T. Laurila, V. Vuorinen, and M. Paulasto-Kröckel, Materials Science and Engineering Reprts, R68, (2010) 1
33. V. Vuorinen, T. Laurila, T. Mattila, E. Heikinheimo, J. Kivilahti, Journal of Electronic Materials 36 (2007) 1355
34. J. Hurtig, Master's Thesis, Helsinki University of Technology, (2006).
35. T. Laurila, J. Hurtig, V. Vuorinen, and J.K. Kivilahti, Microelectronics Reliability 49 (2009) 242